China Geology 7 (2024) 605−629

China Geology

Journal homepage: http://chinageology.cgs.cn
https://www.sciencedirect.com/journal/china-geology

Geological risk assessment of traffic engineering construction among 7.0–8.5 magnitude earthquake areas: Practice from the Sichuan-Tibet transport corridor in the eastern Tibetan Plateau

Ning Zhong[a, b,*], Xian-bing Zhang[c], Chang-bao Guo[a, b,*], Zhen Yang[c], Hao Yu[c], Rui-an Wu[a, b], Yang Wang[a, b], Hai-bing Li[d]

[a] *Key Laboratory of Active Tectonics and Geological Safety*, *Ministry of Natural Resources*, *Institute of Geomechanics*, *Chinese Academy of Geological Sciences*, *China Geological Survey*, *Ministry of Natural Resources* , *Beijing* 100081, *China*

[b] *Research Center of Neotectonism and Crustal Stability*, *China Geological Survey*, *Ministry of Natural Resources*, *Beijing* 100081, *China*

[c] *School of Earth Sciences and Resources*, *China University of Geosciences (Beijing)*, *Beijing* 100083, *China*

[d] *Institute of Geology*, *Chinese Academy of Geological Sciences*, *China Geological Survey*, *Ministry of Natural Resources*, *Beijing* 100037, *China*

ARTICLE INFO

Article history:
Received 30 May 2022
Received in revised form 17 November 2022
Accepted 15 December 2022
Available online 27 September 2023

Keywords:
Earthquake belt
Active fault
Paleoearthquake
Seismicity
Earthquake landslide
Sichuan-Tibet transport corridor
Tectonic deformation pattern
Stress distribution
Geological disater survey engineering
Remote sensing survey

ABSTRACT

At least 13 active fault zones have developed in the Ya'an-Linzhi section of the Sichuan-Tibet transport corridor, and there have been undergone 17 M_S ⩾7.0 earthquakes, the largest earthquake is 1950 Chayu M_S 8.5 earthquake, which has very strong seismic activity. Therefore, carrying out engineering construction in the Sichuan-Tibet transport corridor is a huge challenge for geological technological personnel. To determining the spatial geometric distribution, activity of active faults and geological safety risk in the Sichuan-Tibet transport corridor. Based on remote sensing images, ground surveys, and chronological tests, as well as the deep geophysical and current GPS data, we investigated the geometry, segmentation, and paleoearthquake history of five major active fault zones in the Ya'an-Linzhi section of the Sichuan-Tibet transport corridor, namely the Xianshuihe, Litang, Batang, Jiali-Chayu and Lulang-Yigong. The five major fault zones are all Holocene active faults, which contain strike-slip components as well as thrust or normal fault components, and contain multiple branch faults. The Selaha-Kangding segment of the Xianshuihe fault zone, the Maoyaba and Litang segment of the Litang fault zone, the middle segment (Yigong-Tongmai-Bomi) of Jiali-Chayu fault zone and Lulang-Yigong fault zone have the risk of experiencing strong earthquakes in the future, with a high possibility of the occurrence of M_S ⩾7.0 earthquakes. The Jinsha River and the Palong-Zangbu River, which is a high-risk area for geological hazard chain risk in the Ya'an-Linzhi section of the Sichuan-Tibet transport corridor. Construction and safe operation Ya'an-Linzhi section of the Sichuan-Tibet transport corridor, need strengthen analysis the current crustal deformation, stress distribution and fault activity patterns, clarify active faults relationship with large earthquakes, and determine the potential maximum magnitude, epicenters, and risk range. This study provides basic data for understanding the activity, seismicity, and tectonic deformation patterns of the regional faults in the Sichuan-Tibet transport corridor.

1. Introduction

The Sichuan-Tibet transport corridor (STTC) is located at the eastern margin of the Tibetan Plateau (TP), starting from Chengdu city of Sichuan province in the east and reaching Lasa city of Tibet in the west (Yang ZH et al., 2023; Peng C et al., 2023). The Ya'an-Linzhi section of the STTC is from Ya'an, Kangding, Litang, Changdu, Bomi, to Linzhi (Fig. 1), which has the steepest terrain, the strongest endogenic and exogenic geological processes, and extremely frequent geological disasters in China and even in the world (Guo CB et al., 2020). Presently, the Ya'an-Linzhi section of the STTC is an area with the most complex deformation and well-developed active blocks with numerous active faults (Guo CB et al., 2020; Peng JB et al., 2020). At least 13 active fault

First author: *E-mail address*: zdn2018@126.com (Ning Zhong).

* Corresponding author: *E-mail address*: zdn2018@126.com (Ning Zhong); guochangbao@163.com (Chang-bao Guo).

Literary editor: Xi-jie Chen
doi:10.31035/cg2023055
2096-5192/© 2024 China Geology Editorial Office.

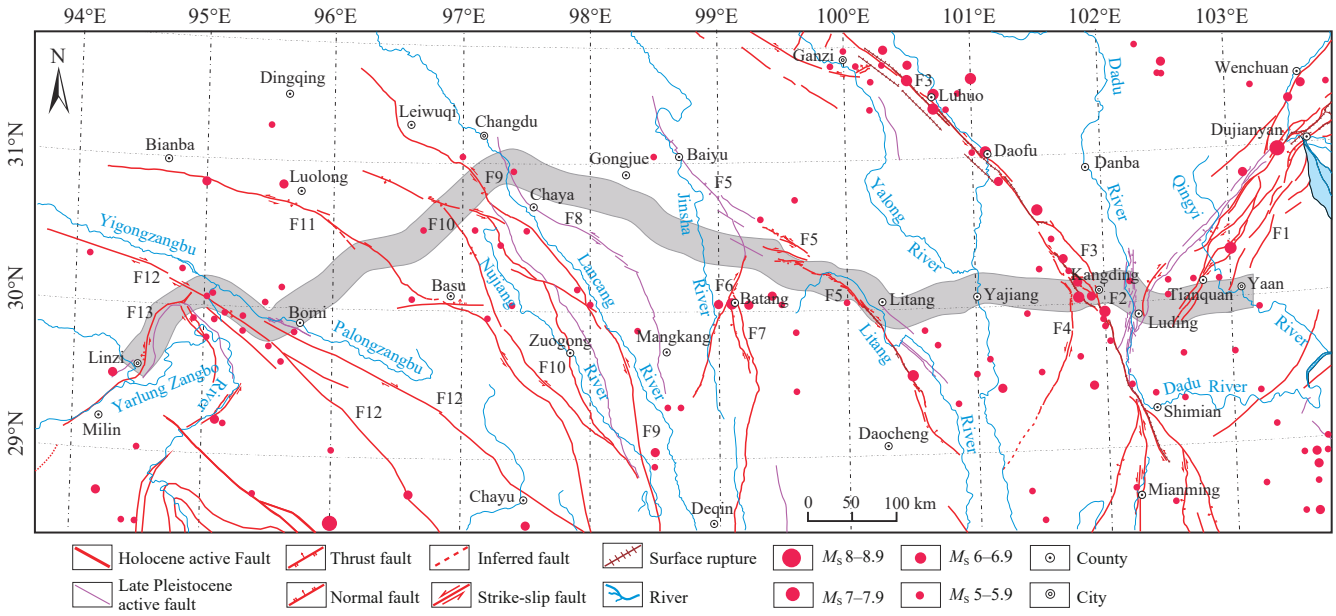

Fig. 1. Distribution map showing major active faults and earthquake epicenters in the Ya'an-Linzhi section of the Sichuan-Tibet transport corridor.

zones have developed in the Ya 'an-Linzhi section of the STTC, including 10 Holocene active fault zones (e.g. Longmenshan, Xianshuihe, Yunongxi, Litang, Batang, Lancangjiang, Nujiang, Bianba-Luolong, Jiali-Chayu, and Lulang-Yigong) and three Late Pleistocene-Holocene active fault zones (e.g. Daduhe, Jinshajiang, and Xiangdui-Luoni), and these active faults are mainly of thrust, strike-slip, thrust-strike-slip, and strike-slip-normal types and are dominated by strike-slip faults (Fig. 1; Table 1). The Ya'an-Linzhi section of the STTC has experienced many large earthquakes since 1948, including the 1948 Litang M_S $7^1/_4$ earthquake, the 1950 Chayu M_S 8.5 earthquake, the 1955 Zheduotang M_S 7.5 earthquake, the 2008 Wenchuan M_S 8.0 earthquake, and the 2013 Lushan M_S 7.0 earthquake, indicating very strong seismicity. Active faults frequently cause earthquakes and geological disasters, produce coseismic dislocations and creep deformation, and form fault fracture zones, which directly threaten the safety of cities and major projects (Zhong N et al., 2022b). For example, emergency field observations after 2008 Wenchuan M_S 8.0 earthquake, which have found obvious coseismic surface ruptures at Shenxigou village (Fig. 2a; Li HB et al., 2008), a lots of landslides and barrier lakes at Qingchuan city (Figs. 2b, c; Tang C and Westen CJV, 2018). In addition, we also found a bridge was destroyed by the 2008 Wenchuan M_S 8.0 earthquake near Yingxiu town (Fig. 2d; Tang C and Westen CJV, 2018), a significant number of tensional ground fissures at Lingguan town which induced by 2013 Lushan M_S 7.0 earthquake (Fig. 2e; Hong HC et al., 2013), crushing damage of buildings at Moxi town were destroyed by the 2022 Luding M_S 6.9 earthquake (Fig. 2f). Meanwhile, during the development of western China, many national major projects were constructed in the Ya'an-Linzhi section of the STTC, including the South-to-North Water Diversion Project and numerous large-scale cascade hydropower stations in the Sanjiang region (Liu FS et al., 2014; Peng JB et al., 2020). Therefore, there is an urgent need to ascertain the seismicity of the Ya'an-Linzhi section of the STTC throughout the geological history, and to assess the time, locations, and regional large earthquakes risks of future. It is necessary to get the activity parameters of regional faults, such as slip rates, paleoearthquake history, the recurrence intervals of strong earthquakes, and the elapsed time of the most recent earthquake events.

The Ya 'an-Linzhi section of the STTC crosses the Minjiang, Dadu, Yalong, Jinsha, Lancang, Nujiang, Parlung Zangbo, and Yigong Zangbo rivers from east to west (Fig. 1). Its landforms are dominated by extremely high mountain glaciers, high-mountain basins, and deeply incised canyons. Geological disasters, such as collapses, landslides, debris flows, and chain disasters are frequently occur in the Ya'an-Linzhi section of the STTC (Guo CB et al., 2020). The alpine and high-altitude areas in the Ya 'an-Linzhi section of the STTC are difficult to access, and the survey and analyze mainly using remote sensing and tectonic geomorphology. Therefore, it is difficult to accurately determine the geometry of the faults in the Ya 'an-Linzhi section of the STTC. For instance, it is controversial for the Zheduotang fault which crosses the Zheduo mountain in the Xianshuihe fault zone, whether consists of the eastern and western branch faults (Pan JW et al., 2020; Bai MK et al., 2021), or only the eastern branch fault (Liang MJ, 2019). Moreover, the activity of the western branch (Zheduotang fault) remains controversial. Besides, the following issues also directly affect the understanding of the faults activity, and especially the deformation process of the active faults in the Ya'an-Linzhi section of the STTC under the lateral extrusion-induced deformation of the TP: (1) the fault traces are unclear in the densely vegetated areas of the high-mountain canyons; (2) frequent disasters, such as collapses, landslides, and debris flows, cause the erosion rate to be greater than the deposition

rate, leading to a decrease in the quantity of the Quaternary sediments, and are dominated by coarse-grained clastic sediments; (3) the lack of Quaternary dating which hinders the determination of the slip rate and the paleoearthquake. The

Table 1. Main active faults in the Ya'an-Linzhi section of the Sichuan-Tibet transport corridor.

No.	Fault name	Main branch faults	Fault property	Activity age	Activity rate/(mm/a)		Large earthquakes (M_S ⩾6.5)	References
					Horizontal	Vertical		
F_1	Longmenshan	Yingxiu-Beichuan	Thrust and/or Dextra	Holocene		1–3	2008 Wenchuan M_S 8.0	Li HB et al., 2008; Chen LC et al., 2014; Xu XW et al., 2017
		Shuangshi-Dachuan	Thrust and/or Dextra	Holocene	5.0	⩽0.5	2013 Lushan M_S 7.0	
		Yanjing-Wulong	Thrust and/or Dextra	Late Pleistocene to Holocene				
		Gengda-Longdong	Thrust					
F_2	Daduhe	Changchang	Thrust	Late Pleistocen				Zhou RJ et al., 2000
		Luding			0.73			
		Detuo						
F_3	Xianshuihe	Ganzi	Sinistral	Holocene	6–8		1854 Ganzi M_S 7.3; 1811 Zhuwo M_S 7.5; 1967 Zhuwo M_S 7.6	Bai MK et al., 2018, 2021; Pan JW et al., 2021
		Luhuo			8–11		1816 Luhuo M_S $7^1/_2$; 1973 Luhuo M_S 7.6	
		Daofu			8–11		1904 Daofu M_S 7.0; 1923 Daofu M_S $7^1/_4$; 1981 Daofu M_S 6.9	
		Qianning			11		1792 Daofu M_S $6^3/_4$; 1983 Daofu M_S 7.0;	
		Yalahe			0.6–2.2		1700 Kangding M_S >6.7;	
		Selaha			3.9–9.9		1748 Kangding M_S $6^3/_4$; 1725 Kangding M_S 7.0	
		south Mugecuo			8–12			
		Zheduotang			3.4–4.8		1955 Zheduotang M_S 7.5	
		Moxi			9.6–13.4		1786 Moxi M_S $7^3/_4$; 2022 Luding M_S 6.9	
F_4	Yunongxi		Sinistral	Holocene				Gao SP, 2021
F_5	Litang	Cuopuhu	Sinistral and normal	Holocene	2.71–3.67		1948 Litang M_S $7^1/_4$	Xu XW et al., 2005; Chevalier ML et al., 2016
		Maoyaba			2.23–2.97			
		Litang			3.05–4.99			
		Kanga-Dewu	Sinistral and thrust		3.83–4.58			
F_6	Batang	Batang	Dextral and thrust	Holocene	2.4 ± 0.3		1989 Batang M_S 6.9;1870 Batang M_S $7^1/_4$	Zhou RJ et al., 2005; Xu XW et al., 2005
		Mangling			2.5–2.7			
F_7	Jinshajiang	Songduo-baiyu	Sinistral and thrust	Late Pleistocen				Zhou RJ et al., 2005
		Batang-Deqin	Dextral and thrust	Holocene				
F_8	Xiangdui-Luoni		Sinistral	Late Pleistocen				This study
F_9	Langchangjiang	Baqing-Leiwuqi	Sinistral and thrust	Holocene	1.2 + 0.5/−0.3	1.2 + 0.4/−0.2		Ren JJ et al., 2022
F_{10}	Nujiang	Yangda-Yaxu	Sinistral and thrust	Holocene	2.2 + 0.6/−0.5	~0.1		Ren JJ et al., 2022; Zhong N et al., 2022b; Han MM, 2022
		Bangda						
F_{11}	Bianba-Luolong		Sinistral and thrust	Holocene			1642–1654 Luolong M ⩾7.0; 1791–1804Bianba M_S $6^3/_4$	Han MM, 2022
F_{12}	Jiali-Chayu	Jiali-Yigong	Dextral and thrust	Holocene	4.6–18.5	2–4	1950 Chayu M_S 8.5	Zhong N et al., 2021
		Yigong-Bomi			1.3–2.0	2.5–2.9		
		Bomi-Chayu			5.1–6.	2–4		
F_{13}	Lulang-Yigong		Sinistral and normal	Holocene	0.4	0.6		Xie C, 2018

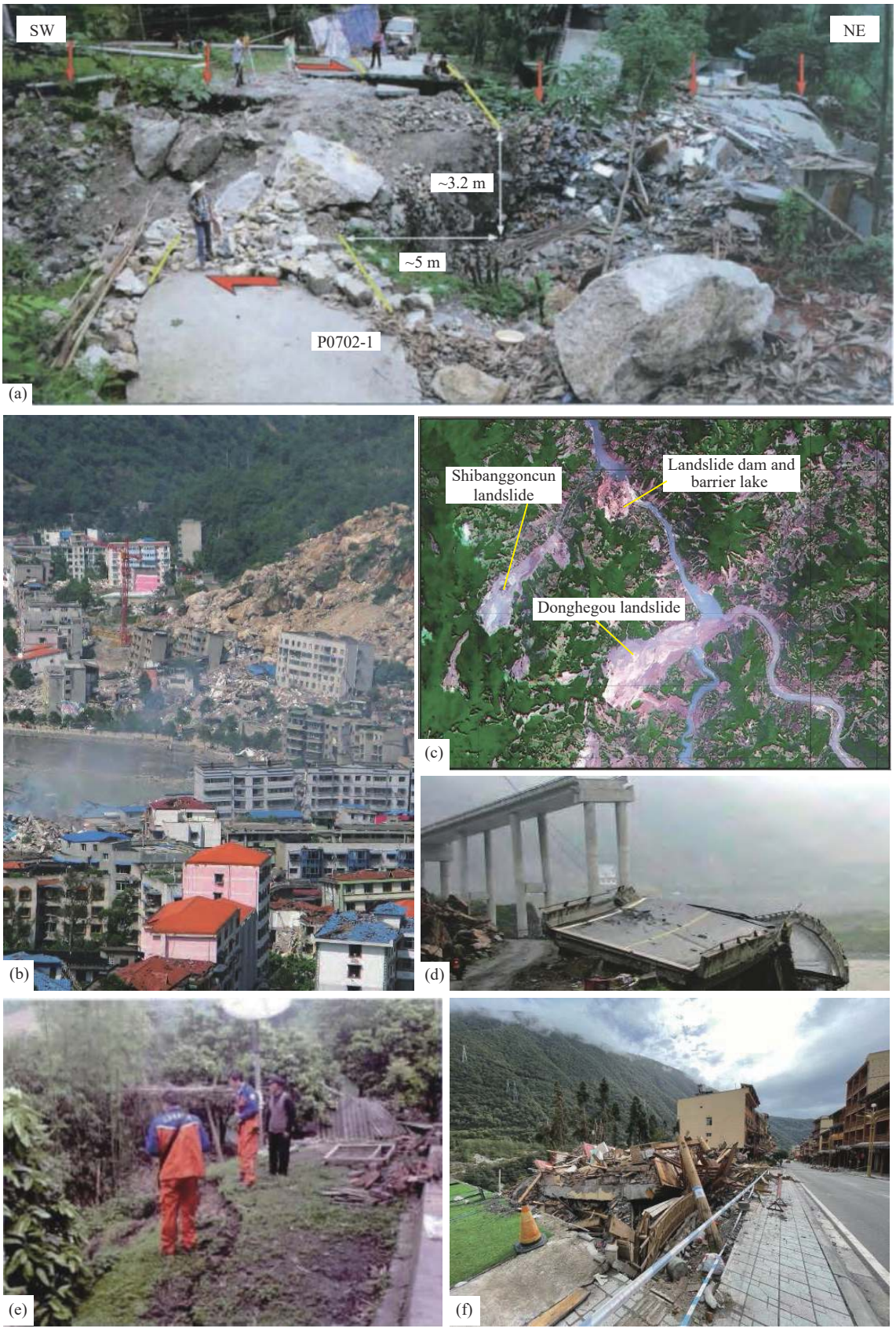

Fig. 2. a–Fracture outcropped in the Shenxigou village, about 3.2 m uplifted road with the about 5 m dextral offset, which generated in the 2008 Wenchuan M_S 8.0 earthquake (Li HB et al., 2008); b– photo of Beichuan county showing the damage caused by the 2008 Wechuan M_S 8.0 earthquake (Tang C and Westen CJV, 2018) ; c–a lots of landslide and barrier lake at Qingchuan county induced by the 2008 Wenchuan M_S 8.0 earthquake (Tang C and Westen CJV, 2018); d–a bridge was destroyed by the 2008 Wenchuan M_S 8.0 earthquake near Yingxiu Town (Tang C and Westen CJV, 2018); e–an arc tissue at Lingguan town generated in the 2013 Lushan M_S 7.0 earthquake around the rural building (Hong HC et al., 2013); f–crushing damage of buildings at Moxi town were destroyed by the 2022 Luding M_S 6.9 earthquake.

spatial geometric distribution and nature of the active faults in the Ya'an-Linzhi section of the STTC (e.g., the central-south segment of the Jiali-Chayu fault zone) are still controversial (Armijo R, 1989; Shen J et al., 2003; Zhong N et al., 2021).

The aim of this study is to (1) reveal the Late Quaternary activity and paleoearthquake records of the faults in the high-mountain basins (the Xianshuihe and Litang fault zones), and in the high-mountain canyons (the Batang, Jiali-Chayu, and Lulang-Yigong fault zones); and (2) explore the deformation mechanisms and tectonic attributes of active faults under the condition of the lateral extrusion-induced deformation of the TP. This study is expected to provide basic data for the evaluation of seismicity and the geological safety of major engineering in this Ya'an-Linzhi section of the STTC.

2. Late Quaternary activity and paleoearthquake history of major fault zones

2.1. Xianshuihe fault zone

2.1.1. Late Quaternary activity of the Xianshuihe fault zone

The Xianshuihe fault zone is located at the boundaries of the intensely active Bayan Har and Sichuan-Yunnan subblocks within the TP (Fig. 3a). It is a large active sinistral strike-slip fault formed by the uplift of the TP and the SE-trending extrusion of the Sichuan-Yunnan block since the Cenozoic (Bai MK et al., 2018, 2021). The Xianshuihe fault zone extends from Kasu, Ganzi in the NW to southern Tianwan, Shimian after passing through Luhuo and Kangding in the SE direction (Fig. 3b), with a total length of approximately 400 km (Li TS et al., 1995; Xiong TY et al., 2010). The Xianshuihe fault zone is composed of nine branch faults, namely the Ganzi, Luhuo, Daofu, Qianning, Yalahe, Selaha, south Mugecuo, Zheduotang, and Moxi faults, which have an en-echelon distribution, Holocene active epoch, and slip rate of 8–10 mm/a (Bai MK et al., 2018; Pan JW et al., 2020). The Yalahe, Selaha, south Mugecuo, Zheduotang, and Moxi faults had slip rates of 0.6–2.2 mm/a, 3.9–9.9 mm/a (9.6–9.9 mm/a for the NW segment and 3.9–4.9 mm/a for the SE segment), 8–12 mm/a, 3.4–4.8 mm/a, and 9.6–13.4 mm/a, respectively, during the Late Quaternary (Bai MK et al., 2021). Ma J et al. (2020) found new evidences for the Holocene activity of the NW-trending segment of the Zheduotang fault through image interpretation, field geological surveys and trenching, and shows that the last paleoearthquake in the Zheduotang fault occurred at 5821±49 B.P., which extends for additional 15 km northwestward compared with previous study results (Li TS et al., 1997). Remote sensing and field investigation, we found two branches faults of the Zheduotang fault in the Zheduotang village, and forming a pull-apart structure (Fig. 4a). The surface fracture formed by the 1955 Zheduotang M_S 7.5 earthquake was clearly visible (Figs. 4b, c). Through the geological, geomorphic interpretations of high-resolution satellite images and detailed tectonic geological mapping in the field, Pan JW et al. (2020) found a new Holocene active fault (south Mugecuo) with a length of about 24 km in the Zheduoshan granite pluton between the Selaha and Zheduotang faults (Fig. 3). They found that south Mugecuo fault can be spatially divided into northern, central, and southern segments in a (normal-slip) sinistral and right-stepping en-echelon pattern (Pan JW et al., 2020). Since 1725, the Xianshuihe fault zone has undergone nine M_S 7.0 earthquakes, one earthquake of M_S 6.9, and 15 earthquakes of M_S 6.0–6.8, with a recurrence interval of large earthquakes of about 30 years (Bai MK et al., 2021). The most recent earthquake in the Xianshuihe fault zone is Luding M_S 6.8 earthquake, which occurred on September 5, 2022.

2.1.2. Future seismic hazard segements of the Xianshuihe fault zone

Based on surveys of active faults and paleoearthquake studies, it has been found that the Selaha area in the Luhuo-Kangding segment of the Xianshuihe fault zone is a seismic gap (Liang MJ, 2019). As shown by the coseismic and postseismic Coulomb stress disturbances of the 2014 Kangding M_S 6.3 earthquake, the Kangding segment of the Xianshuihe fault zone is characterized by severe stress accumulation (Li DH et al., 2015). Xu J et al. (2017) analyzed the cumulative change in the Coulomb stress caused by the coseismic and postseismic effects of the 1976–2017 earthquakes at the eastern margin of the TP, including the 2008 Wenchuan M_S 8.0 earthquake, the 2013 Lushan M_S 7.0 earthquake, and the 2017 Jiuzhaigou M_S 7.0 earthquake, and found that the Coulomb stress increased significantly in the south-central Xianshuihe fault zone, especially in the Selaha segment, indicating the increased urgency of seismogenic hazards. Although the 2014 Kangding M_S 6.3 earthquake occurred in the Kangding segment, it did not completely release the cumulative stress in this segment (Xiong W et al., 2016). Since 1900, the TP has undergone three high-frequency periods of earthquake clustering, with an active period of strong earthquakes of approximately 30 years (Deng QD et al., 2014). The current Kunlun-Wenchuan earthquake series (e.g., the 2001 Kunlun M_S 8.1 earthquake and the 2008 Wenchuan M_S 8.0 earthquake) was mainly active in the Bayan Har block. Deng QD et al. (2014) emphasized that special attention should be paid to the possibility of the occurrence of M_S 7–8 earthquakes in the Bayan Har block. In addition, small earthquakes occurred frequently along the south-central Xianshuihe fault zone from 2001 to 2022, especially after the 2014 Kangding M_S 6.3 earthquake (Yi GX et al., 2015) and 2022 Luding M_S 6.8 earthquake (Zhang L et al., 2022). The Xianshuihe fault zone is located at the junction between the Bayan Har block and the Sichuan-Yunnan block, which is the part of the TP that is extruded southeastward. Moreover, the Yalahe fault is in a transitional stage area, where the stress is prone to accumulate. The Bayan Har block is a pivot area where the direction of the crustal movement in the TP shifts. In the north of the Bayan Har block, strong compressional uplift generally occurs at the northeastern margin of the TP, in contrast, the southern Bayan Har block is dominated by eastward extrusion (Li HB et al., 2021). With such strong

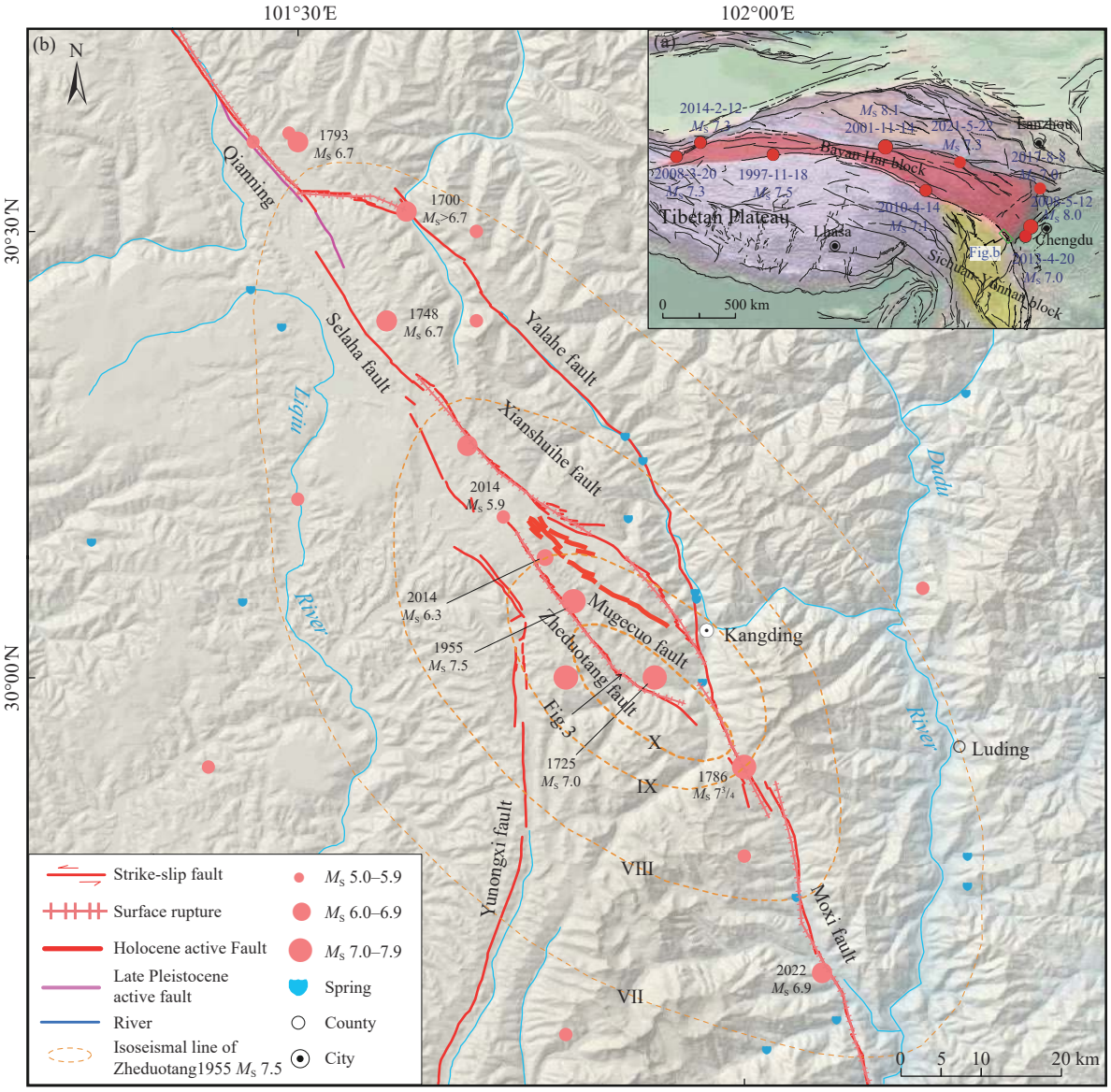

Fig. 3. a–Distribution of M_S≥7.0 earthquakes since 2001 in the Bayan Har block and its periphery; b–map showing the spatial geometric distribution and historical earthquakes in the Selaha-Kangding segment of the Xianshuihe fault zone and the isoseismal distribution of the 1955 Zheduotang M_S 7.5 earthquake (after Tang RC and Han WB, 1993).

crustal deformation, the fault zone around the Bayan Har block is particularly active (Cheng J et al., 2018). It has been 298 years and 78 years since the occurrence of the 1725 Kangding earthquake and the 1955 Zheduotang earthquake, respectively. With a slip rate of about 10 mm/a, the Xianshuihe fault zone has a cumulative displacement of 0.78–2.98 m. Based on the relationship between coseismic displacement (D) and magnitude expressed as M = 6.81 + 0.78 log (D) (Deng QD et al., 1992), it can be estimated that the magnitude of the next earthquake will be M_S 6.7–7.2. It has been 22 years since the 2001 Kunlun M_S 8.1 earthquake. From the 30 years active period of the Kunlun-Wenchuan earthquake series, it can be inferred that the Selaha area in the Luhuo-Kangding segment has the conditions for the occurrence of M_S 7.0 earthquakes in the future. Based on investigation, historical earthquakes, the strike-slip rates of the faults since the Late Quaternary, and empirical equations for the maximum displacement and magnitude of earthquakes, Bai MK (2022) proposed that the Selaha fault and Moxi fault in the southeastern segment of the Xianshuihe fault zone are at risk of experiencing earthquakes of M_w 6.7–7.0, M_w 7.0–7.1, respectively in the future. Bai MK (2022) also suggested the Mugecuo-Selaha area in Kangding is prone to form earthquake nucleation due to the presence of the Mugecuo pull-apart structure. In particular, the 2021 Maduo M_S 7.4 earthquake caused the strain release of the northern boundary of the Bayan Har block, which may lead to a new accumulation of strain at the southern boundary of the block (Pan JW et al., 2021). The coseismic Coulomb stress in the Kangding area has increased significantly since 2022 Luding M_S 6.8 earthquake (Zhang L et al., 2022). Therefore, the activity and risk of strong earthquakes in the Xianshuihe fault zone have increased, especially Selah-Kangding segment.

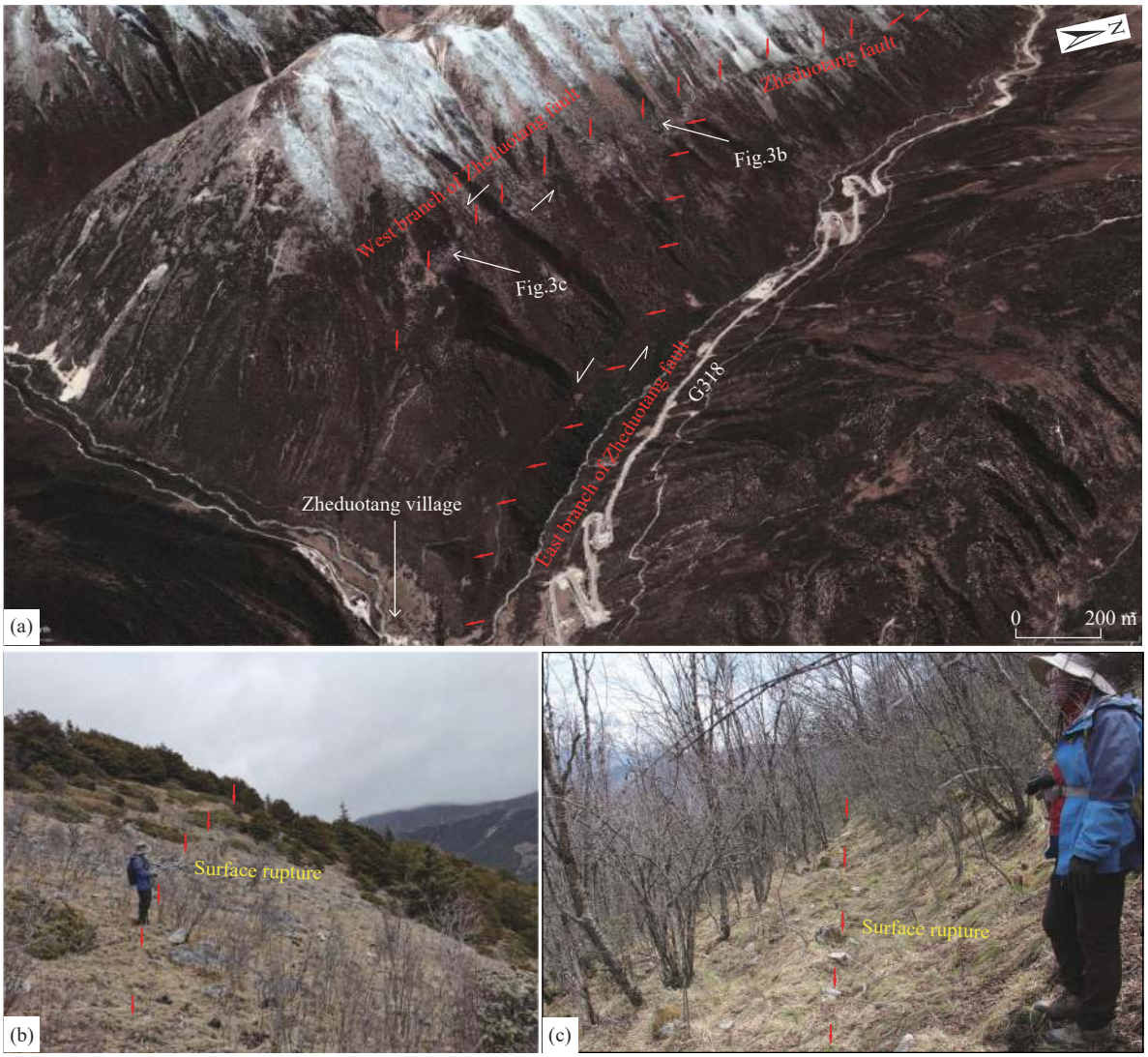

Fig. 4. Spatial geometric distribution of the Zheduotang fault, and surface ruptures caused by 1955 Zheduotang M_S 7.5 earthquake.

2.2. Litang fault zone

2.2.1. Late Quaternary activity of the Litang fault zone

The Litang fault zone is a sinistral strike-slip active fault in the central part of the Sichuan-Yunnan block, and is nearly parallel to the Xianshuihe and Honghe fault zones (Figs. 5a, b), which regulates the eastward extrusion of the southeastern margin of the TP (Tang RC and Han WB, 1993; Zhang YZ et al., 2015; Chevalier ML et al., 2016; Li HB et al., 2021). The Litang fault zone starts Xiebacun at Baiyu county in the northwest and ends in northern Muli county after extending southeastward through the Cuopuhu, Maoyaba, Litang, Jiawa, and Dewu areas, with a total length of approximately 465 km. The Litang fault zone is a Holocene active fault composed of five secondary faults, namely Cuopuhu, Maoyaba, Litang, Kangga-Dewu and Shawan (Xu XW et al., 2005; Zhou RJ et al., 2014; Chevalier ML et al., 2016). The Litang fault zone exhibits significant Cenozoic activity, and its Paleogene-Quaternary strata are generally subjected to folding or faulting (Zhou RJ et al., 2014). It hosts linearly distributed hot springs, as well as significant water streams and ridge offset (Zhao GH, 2014) and noticeable earthquake surface rupture in the Litang fault (Figs. 6a–d). The most recent earthquake in the Litang fault zone is the 1948 Litang M_S $7^1/_4$ earthquake, which ruptured the Litang segment and the Kangga-Dawu segment simultaneously with a total length of about 36–70 km, and had maximum coseismic sinistral and vertical displacements of 4.3 m and 1 m, respectively (Liu K et al., 2021; Xu XW et al., 2005; Zhou CJ et al., 2015). During the Holocene, the Litang fault zone had average horizontal slip rates of 3.2–4.4 mm/a in Litang segment and 2.6–3.0 mm/a in north of Litang, respectively, and an average vertical slip rate of 0.1–1.8 mm/a (Xu XW et al., 2005). Moreover, the Late Pleistocene-Holocene horizontal slip rates of the Cuopuhu segment, the northern margin of Maoyaba, the Litang segment, and the Kangga-Dawu segment were 2.71–3.67 mm/a, 2.23–2.97 mm/a, 3.05–4.99 mm/a, and 3.83–4.58 mm/a, respectively (Xu XW et al., 2005; Chevalier ML et al., 2016).

2.2.2. Recurrence characteristics of paleoearthquakes of the Litang fault zone

The Maoyaba Basin is the largest basin in the Litang fault zone, with a length of about 30 km and a width of up to 10

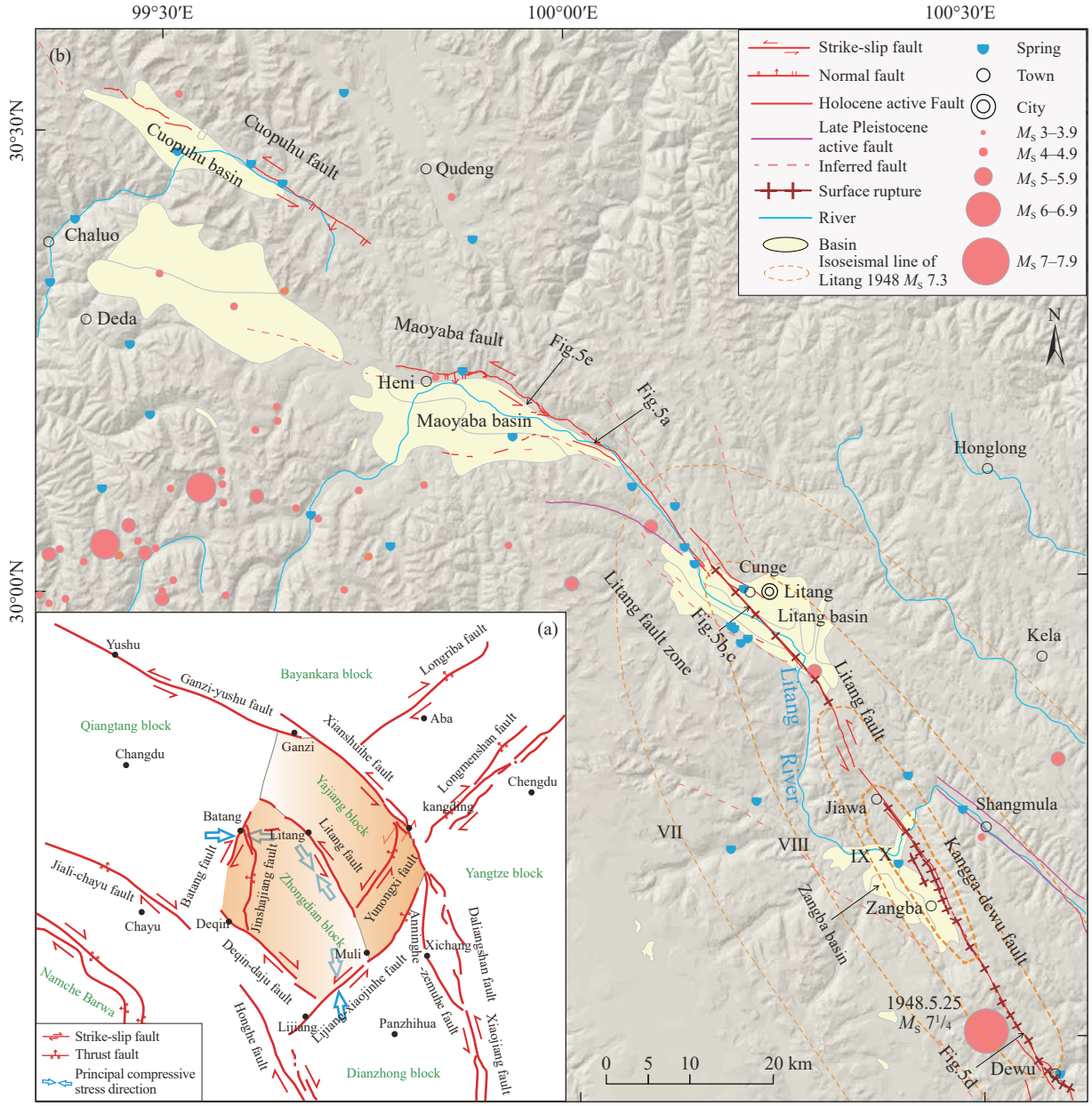

Fig. 5. a–Distribution map showing major active faults and internal deformation pattern of subblocks in northwestern Sichuan (after Gao SP, 2021); b–map showing the spatial geometric distribution and historical earthquakes in the Litang fault and the isoseismal distribution of the 1948 Litang earthquake of M_S $7^1/_4$ (after Tang RC and Han WB, 1993).

km. The major boundary faults (i.e., the northern and southern boundary faults) of the Maoyaba Basin are all Holocene active faults (Zhao GH, 2014), and large earthquakes that ruptured the surface have occurred in the major boundary faults since the Late Holocene (Xu XW et al., 2005; Zhou RJ et al., 2014; Chevalier ML et al., 2016; Guo CB et al., 2016). For instance, a moderate-strong earthquake occurred in the northern boundary fault at about 119±2 years, with surface rupture traces still existing (Xu XW et al., 2005). It has been widely accepted that the Luanshibao landslide was caused by a seismic event (Fig. 6e), which due to active of the northern boundary Maoyaba fault (Wang JT et al., 2023). The dating results show that the Luanshibao landslide has strong activities at 9400 B.P., 3510 ± 346 B.P., 1980 ± 30 B.P., 993 ± 45–1057 ± 45 B.P., and 125 ± 25 B.P., respectively (Guo CB et al., 2016; Zeng QL et al., 2020; Wang JT et al., 2023), suggesting that the Luanshibao landslide have multiple stages of activity, indicates that the area has strong seismic activity. As shown by many previous studies, the northern boundary fault of the Maoyaba Basin mainly exhibits sinistral strike-slip components (Deng QD et al., 2009; Zhang D et al., 2019), followed by normal fault components (Wu ZH et al., 2014; Zhang YZ et al., 2015; Chevalier ML et al., 2016), with a vertical rate of 0.6 ± 0.1 mm/a. What 's more, some researchers believed that the northern boundary fault of the Maoyaba Basin has thrust components (Xu XW et al., 2005). As for the southern boundary fault of the Maoyaba Basin, a few studies have been conducted (Zhou RJ et al., 2005), and its geometric distribution was yet to be investigated in detail. According to the published data, three paleoearthquake

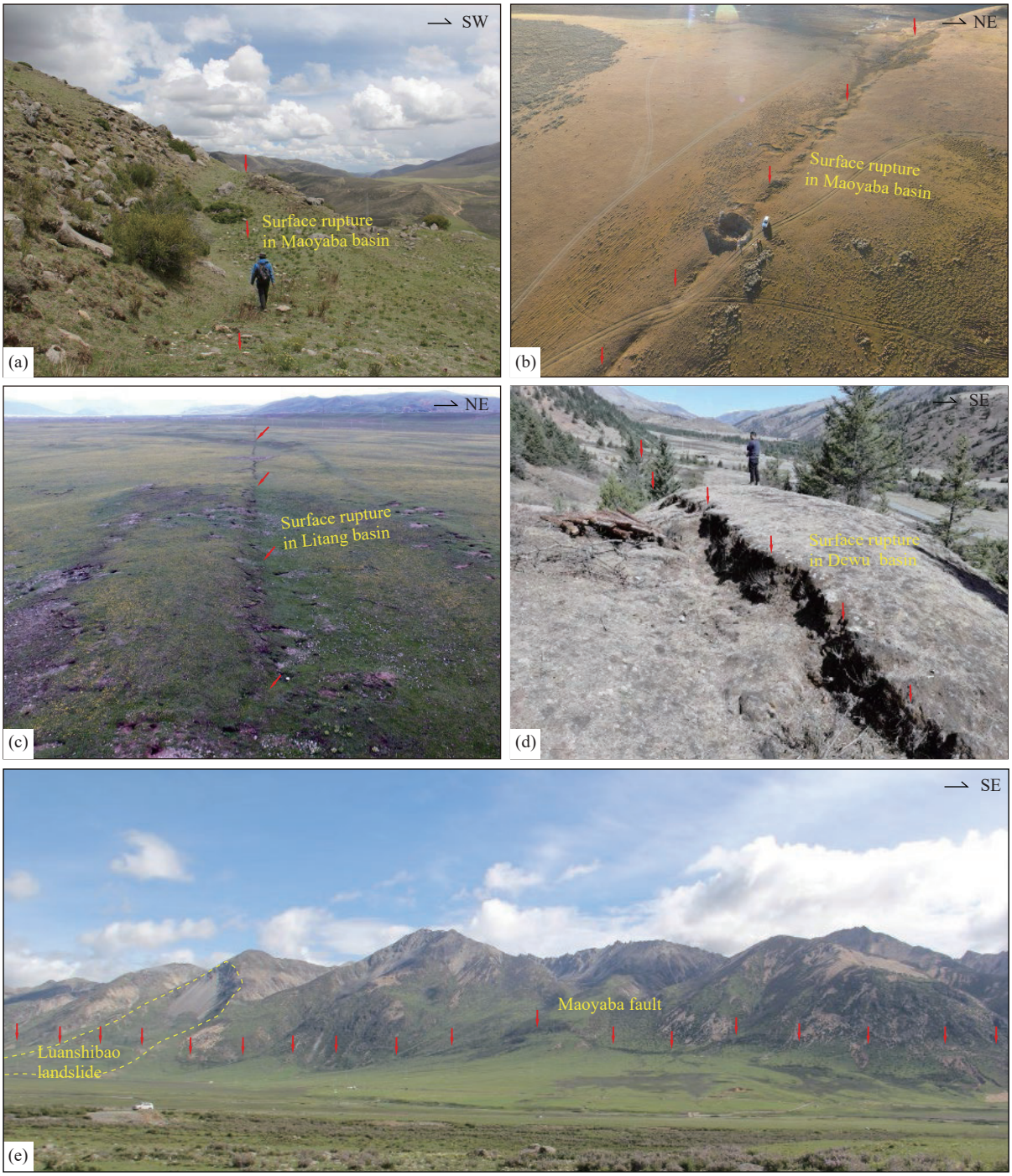

Fig. 6. Surface ruptures caused by historical earthquakes in the Litang fault zone (a–d), and the spatial geometric distribution of the Maoyaba fault (e).

trenches have been excavated at each of the northern and southern boundary faults of the Maoyaba Basin. Six paleoearthquake events have been identified in the trenches excavated in the northern boundary fault, namely E1 (10450–8895 B.P.), E2 (5260–4415 B.P.), E3 (3385–2905 B.P.), E4 (2180–1880 B.P.), E5 (528–482 B.P.), and E6 (64 B.P.) (Fig. 7a); and three events have been identified in the trenches of the southern margin fault, namely E1 (2180±49 B.P.), E2 (957±45 B.P.), and E3 (1890) (Zhou RJ et al., 2016; Zhao GH, 2014; Ren JJ et al., 2021). Paleoearthquake studies indicate that at least seven strong earthquake events might have occurred in the Litang fault (Xu XW et al., 2005; Zhao GH, 2014; Zhou CJ et al., 2015; Zhang KQ et al., 2020; Gao SP, 2021), namely E1 (10680–10250 B.P.), E2 (9483–9191 B.P.), E3 (5358–4750 B.P.), E4 (3418–3307 B.P.), E5 (2030–1930 B.P.), E6 (1380–483 B.P.), and E7 (AD 1729 or 1948), with recurrence intervals of 1128 years, 4283 years, 1692 years, 1382 years, 1271 years, and 798 years, respectively (Fig. 7b). At least five paleoearthquake events have occurred in the Kangga-Dewu fault (Gao SP, 2021), namely E1 (8800–7242 B.P.), E2 (6680–5706 B.P.), E3 (5099–4482 B.P.), E4 (1567–665 B.P.), and E5 (AD1948)

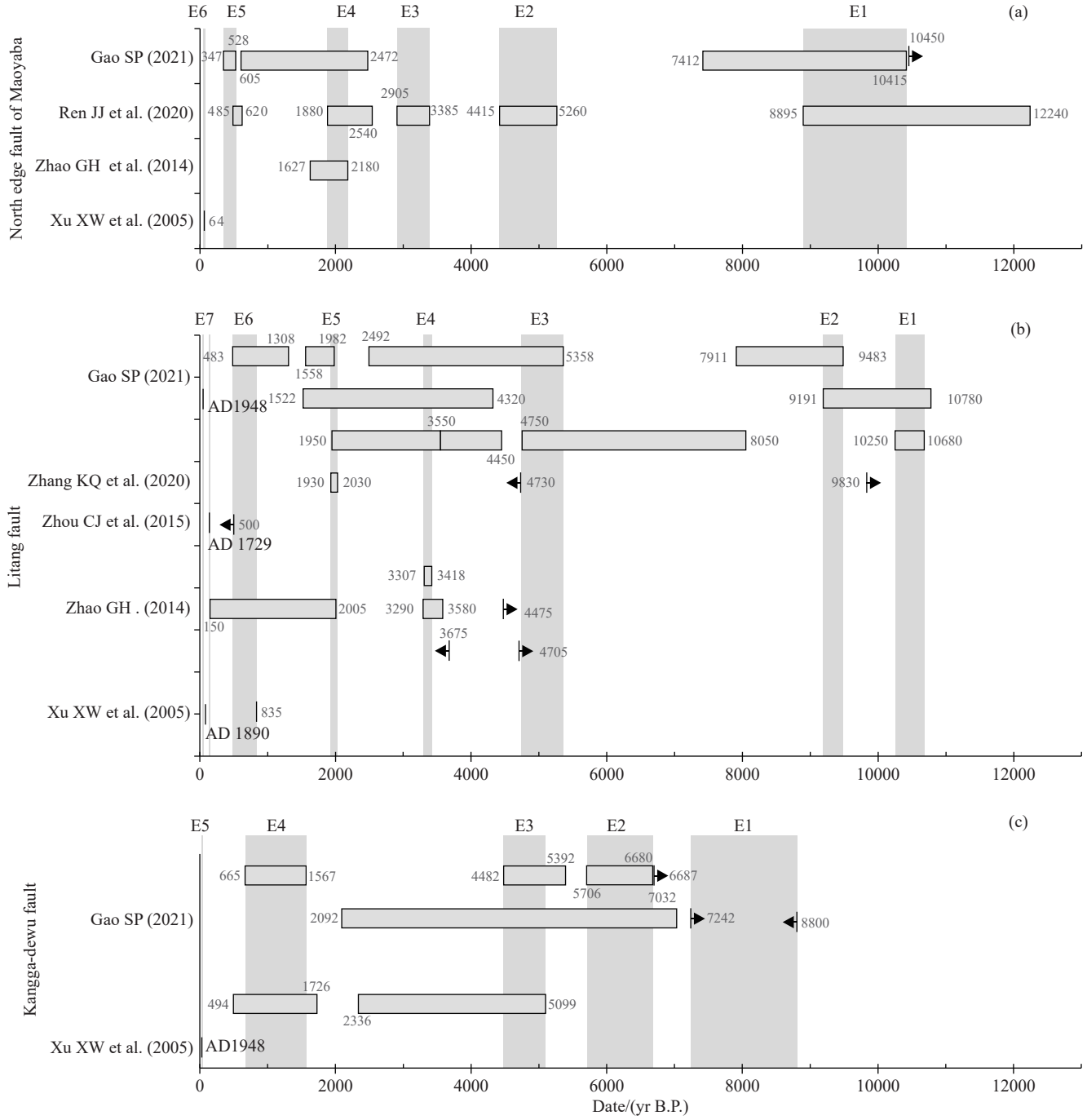

Fig. 7. Paleoearthquake events in the northern boundary fault of the Maoyaba Basin, the Litang fault, and the Kangga-Dewu fault since the Holocene.

(Fig. 7c). The paleoearthquake data on the northern boundary fault of Maoyaba Basin, the Litang fault, and the Kangga-Dewu fault since the Holocene indicate the non-characteristic rupture behavior of the rupture events in the Litang fault zone (Fig. 7). Gao SP et al. (2022) also believed that the rupture events in the Litang fault zone showed non-characteristic rupture behavior and continuous migration of the fault zone along the rupture. Besides, Gao SP et al. (2022) believed that the three faults (northern boundary fault of Maoyaba Basin, Litang fault and Kangga-Dewu fault) underwent roughly the same number of rupture events, leading to an even stress release. The paleoearthquake data since the Holocene show that the time spans of the northern boundary fault of Maoyaba Basin, the Litang fault, and the Kangga-Dewu fault in the Litang fault zone have been rapidly reduced from about 6000 to 1800 years and then to 520 years, and this result indicates that the activity of the Litang fault zone has continuously increased (Gao SP, 2021). In addition, the Litang fault may have a quiet period of about 4000 years during 5000 to 9000 years. After 5000 years, the Litang fault entered a new round of earthquake clustering, and the recurrence intervals of strong earthquakes gradually decreased, indicating an accelerating trend. Therefore, special attention should be paid to the risk of strong earthquakes on the Litang fault.

2.2.3. Future seismic hazard segements of the Litang fault zone

Since 1900, the TP has experienced earthquake clustering peaks three times, namely Haiyuan-Gulang in 1920–1937, Chayu-Dangxiong in 1947–1976, and Kunlun-Wenchuan from 1995, which primarily occurred in the Bayan Har block (Deng QD et al., 2014). Therefore, in the next few years following the last earthquake clustering, attention should be paid to the possibility of the occurrence of M_S 7.0 earthquakes at the eastern margin of the TP, especially in the Bayan Har block and the south-central parts of the northern and southern earthquake belts (Deng QD et al., 2014). The seismicity around and within the Bayan Har block has attracted increasing attention, especially with the occurrence of the 2013 Lushan M_S 7.0 earthquake, the 2017 Jiuzhaigou M_S 7.0 earthquake, and the 2021 Maduo M_S 7.4 earthquake. Moreover, both the 2021 Maduo M_S 7.4 earthquake (Zhan Y et al., 2021) and the 1947 Dari M_S $7^3/_4$ earthquake (Liang MJ et al., 2020) occurred within the Bayan Har block, and formed significant coseismic surface rupture zones 151 km and 70 km, respectively. This result indicates that significant deformation also occurred within the Bayan Har block when the block was extruded eastward overall. According to Gai HL et al. (2021), the Bayan Har block is an atypical rigid block, some of its deformations were absorbed and regulated by its internal diffuse deformations, although its movement and deformations were mostly regulated by the major boundary faults. Therefore, the Bayan Har block is the combined result of rigid block extrusion and diffuse deformation. The 1948 Litang M_S $7^1/_4$ earthquake occurred in western Sichuan, which is the largest strike-slip earthquake in the rhombic Sichuan-Yunnan block in nearly a century, with an existing surface rupture length of 36–70 km (Liu K et al., 2021; Xu XW et al., 2005; Zhou CJ et al., 2015). Based on the seismic stress drop is significantly higher in the northwestern segment of the Litang fault than in its southeastern segment, and the frequency of small earthquakes is higher in the former than in the latter, Wu WW et al. (2017) suggested the Litang fault zone weakens gradually from the northwest to the southeast, and that the relatively closed NW segment (Maoyaba) of the banded fault structure is more prone to accumulate strain and poses greater seismic risks than its other segments. Based on the rupture gaps of strong earthquakes determined using seismogeological data, the segments with locked fault movement revealed using geodetic surveys, the segments with sparse medium-small earthquakes determined using earthquake activity, and the segments with significantly enhanced Coulomb stress determined using numerical simulations, Shao ZG et al. (2022) comprehensively concluded that the boundary zones of the active blocks in China continent may lie in the major fault segments during the late interseismic periods. Moreover, they also preliminarily believed that the Maoyaba segments of the Litang fault zone have high risk coefficients of earthquakes (Shao ZG et al., 2022).

2.3. Batang fault zone

2.3.1. Late Quaternary activity of the Batang fault zone

The Batang fault zone is located at the junction between western Sichuan. Starting near Moxi in the northeast, the Batang fault zone extends southwestward through Songduo, Moduo, Huangcaoping, Batang, and continues to extend southwestward through Zhubalong and Mangling after passing the Jinsha River, and finally wedges out along the Lanchang River (Fig. 8). The Batang fault zone has a total length of about 200 km, an overall strike of NE30°, a dip direction toward the NW, and a steep dip angle. Moreover, the Batang fault zone is dominated by dextral strike-slip motions and obliquely intersects the Jinshajiang fault zone over a length of about 20–30 km. Hot springs are densely distributed along the Batang fault zone, such as the Chaluo hot springs are well known as the largest high-temperature gas spring group in Sichuan (Zhou RJ et al., 2005). A series of paleoearthquake landslides are developed along the Batang fault zone, such as the Chashushan landslide (Zhang YS et al., 2023) and the Songduoxiang landslide (Fig. 9a–c; Yang ZH et al., 2021), showing strong activity of the Batang fault zone. The Batang fault zone has exhibited significant activity since the Late Quaternary, which underwent the 1870 Batang M_S $7^1/_4$ earthquake, the surface rupture traces are still faintly visible on the modern proluvial fan in the Huangcaoba area in northern Batang, such as some reverse fault scarps with a height of only 0.6 ± 0.2 m (Xu XW et al., 2005). Moreover, the 1870 Batang M_S $7^1/_4$ earthquake had a coseismic dextral strike-slip displacement of about 1.5 m (Xu XW et al., 2005, 2017). The 1989 Batang and Litang M_S 6.7 earthquake swarms are also closely related to the activity of the Batang fault zone (Zhou RJ et al., 2005). In addition, in the fault profile encountered at a tunnel portal of the Lala Mountain in Moduo, Batang, the fault offsets the layer U3 composed of gabbros and cataclasites, the sandy mudstone layer U2, and the overlying humus layer (U1) until the surface. This offset phenomenon may represent the surface rupture caused by the 1870 Batang M_S $7^1/_4$ earthquake (Figs. 9d, e).

Based on the gully offsets and thermoluminescence dating of the proluvial fans in Mangling, Mangkang and Batang in TP, Zhou RJ et al. (2005) found that the Mangling and Batang segments of the Batang fault zone had a slip rate of 2.5–2.7 mm/a and 1.3–1.9 mm/a, respectively, since the Late Quaternary. According to the analysis of offset landforms, Xu XW et al. (2005) constrained the average Holocene dextral strike-slip and vertical slip rates of the Cuosanglong area in the northern segment of the Batang fault zone to be 6.7 ± 1.8 mm/a and 2.4 ± 0.3 mm/a, respectively. Overall, the activity of the Batang fault zone appears to be gradually weakening from SW to NE. This finding may be related to the following two facts (Zhou RJ et al., 2005): (1) The southwestern segment of the Batang fault zone is located in the eastern TP block, which had a higher slip rate than the western Sichuan block; (2) there were very complex intersection relationships between the northeastern segment of the Batang fault zone

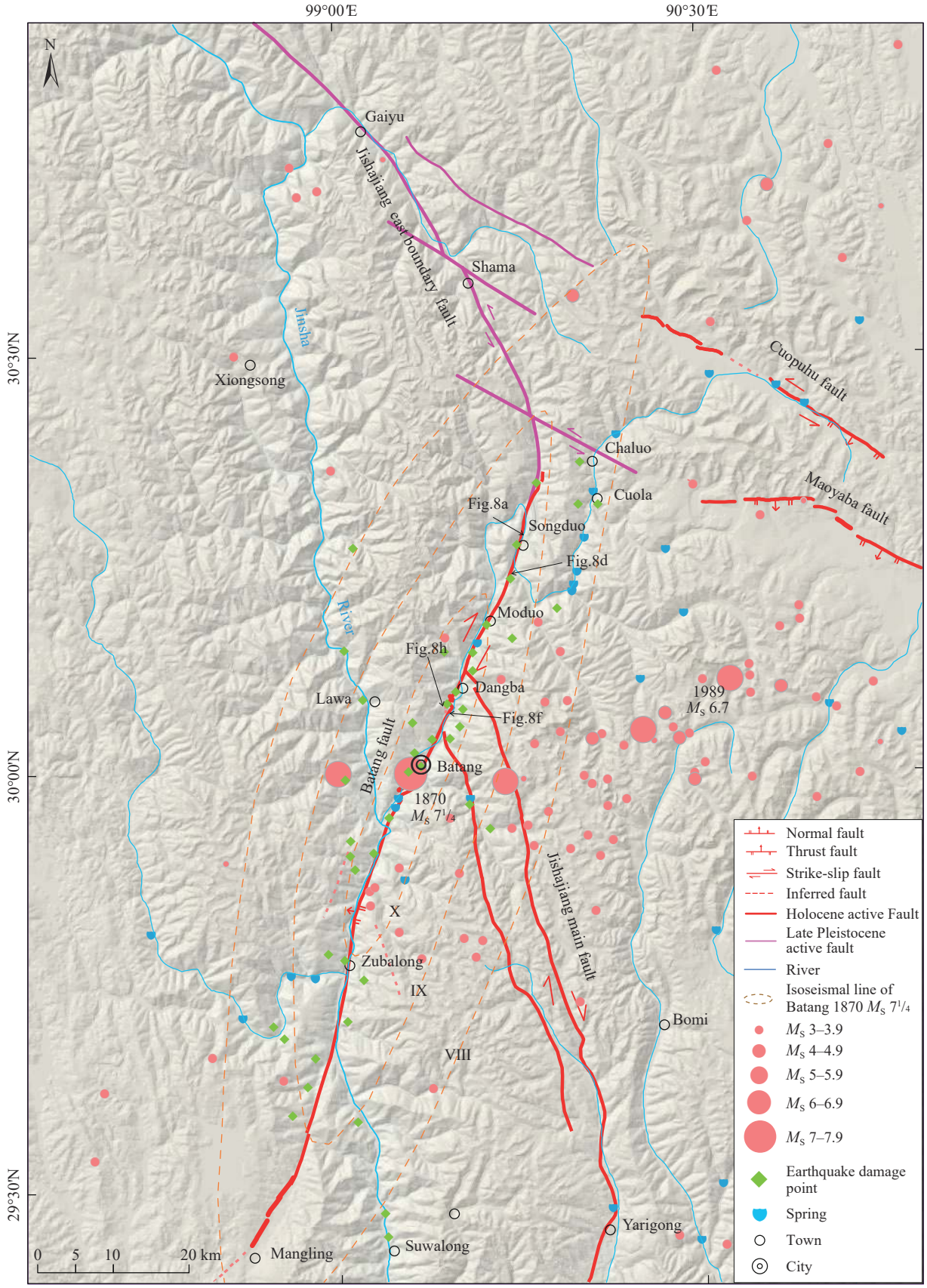

Fig. 8. Map of the spatial geometric distribution and historical earthquakes in the Batang fault zone and the isoseismal distribution of the 1870 Batang M_S 7¼ earthquake (after Tang RC and Han WB, 1993).

and the Jinshajiang fault zone, and thus a part of the motion potential of the former may have been absorbed by the latter.

2.3.2. Paleoearthquakes history of the Batang fault zone

A layer of pseudonodules deformation structures has been

found in the lacustrine sediments at a portal of the Huangcaoping No. 1 Tunnel in Batang. This layer is sandwiched between the upper and lower undeformed layers and extends laterally for more than 10 m. A sample for dating by optically stimulated luminescence (OSL) was collected about 10 cm below the bottom of this layer, and its age was constrained to 5.93 ka (Figs. 9f-g; Table 2). No deformation structures caused by landslides or slope gravity (Zhong N, 2017) or flooding (Zhong N et al., 2020) are visible in the profile. Based on the identification criteria for the seismic origin of the soft−sediment deformation structure (SSDS), the pseudonodules were considered to be caused by the falling of light-gray silty mud into light-yellow fine-grained sands under strong seismic vibration (Zhong N et al., 2019), thus representing an earthquake event after 5.93 ka. According to the characteristics of the pseudonodules, including its deformation type, morphology, and intensity change, as well as its distance from the seismogenic fault (Zhong N, 2017; Zhong N et al., 2017a, 2022a), it can be determined that the pseudonodules indicate an earthquake with a magnitude of about *M* 7.0. In addition, faults F5, F4, and F2 encountered in the Huangcaoping trench in Batang all offset the layer U3, revealing a paleoearthquake event that occurred at about 5110 ± 30 B.P. (Fig. 9h; Gao SP, 2021). Xiang W (2023) excavated

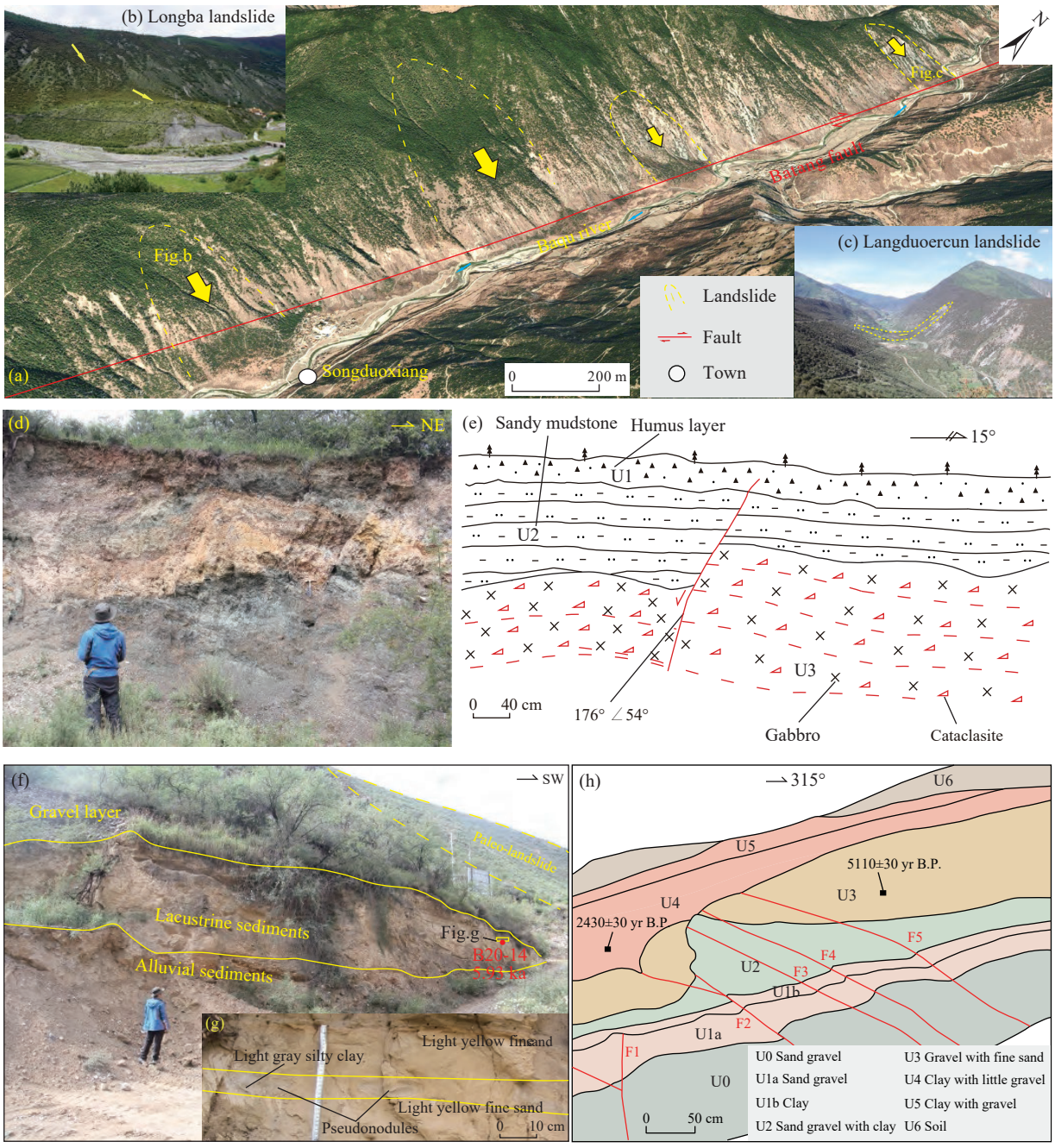

Fig. 9. a–Characteristics of typical seismic landslides in the Batang fault zone (modified from Yang ZH et al., 2021); b–Longba landslide; c–Langduoercun landslide; d, e–Fault profile at a tunnel of the Lala mountain tunnel in Batang; f, g–deformation of seismogenic SSDS recorded by lacustrine deposits at one portal of the Huangcaoping No. 1 Tunnel; h–Huangcaoping paleoearthquake trench (after Gao SP, 2021).

Table 2. OSL dating results for the Huangcaiping, Tongmai, Bitongcun and Dongjiucun sections.

Sample	Site	Depth /m	U /(μg/g)	Th /(μg/g)	K/%	Water content /%	Grain size /μm	Method	Equivalent dose /(Gy/ka)	Dose rate /(Gy/ka)	Age/ka
B20–14	Huangcaoping	3.4	2.52±0.06	11.7±0.07	1.89±0.01	5.27	90–125	SAR	3.31±0.13	19.62±1.22	5.93±0.44
*SCZ01–04	Tongmai	6	3.08±0.09	14.5±0.44	2.73±0.08	16.89	90–125	SAR	4.63±0.31	70.97±5.54	15.33±1.58
*B2019–2	Bitongcun	4.6	2.05	18.8	2.23	5	90–125	SAR	4.11±0.18	35.48±1.93	8.63±0.6
B2019–21	Dongjiucun	7.2	1.77	12.3	2.23	5	90–125	SAR	3.5±0.16	68.52±6.31	19.58±2.01

Note: * OSL dating from Zhong N et al. (2021).

two trenches in Huangcaoping, and identified three paleoearthquake events (E3: 4466–4282 B.P., E2: 357–3264 B.P., E1: 1283 B.P.-present). In summary, a paleoearthquake event with a magnitude greater than *M* 7.0 occurred in the Batang fault zone at 5930–5110 years. Based on the paleoearthquake results obtained through trenching in Moxi (E2, before 844 AD; E3, 839–1405 AD; E4, after 1448 AD), Dangba (E3, before 5489 BC; E4, after 1700 AD), Huangcaoping (E1, before 3716 BC; E2, after 3671–1203 BC; E3, 488–1250 AD; E4, 1585 AD), and Mangling (E3, 11856–7136 BC; E4, after 1426 AD), Gao SP (2021) concluded that the activity of the Batang fault zone was weak during the Early Holocene and then became intensified and transitioned to the clustering stage since the beginning of the AD period, with the earthquake recurrence interval shortening to about 830 years.

2.4. Jiali-Chayu fault zone

The Jiali-Chayu fault zone is the eastern segment of the Karakorum-Jiali fault zone and its eastern extension, starting from southern Naqu in the northwest, extends southeastward through Sangdi, Maidi Zangbo, Azha and then reaches Tongmai along the Yigong-Zangbo River, and then continues to extend southeastward through Chayu along the Gongri-Gabuqu until it leaves China. The Jiali-Chayu zone is considered the southern boundary of the part of the main body of the TP, and extruded substantially eastward, which can be roughly divided into three parts by the Eastern Himalayan Syntaxis (EHS), namely the northwestern segment to the west of the syntaxis, the central Yigong-Tongmai-Bomi segment at the top of the syntaxis, and the southeastern Bomi-Chayu segment to the southeast of the syntaxis (Fig. 10). Based on remote sensing images and geological surveys of the central-south Jiali-Chayu fault zone, as well as research on offset landforms (Figs. 11a–f) and the SSDS of Late Quaternary lacustrine sediments, paleoearthquake trenching and geological dating (Figs. 11g, h), Zhong N et al. (2021) identified two new paleoearthquake events, whose occurrence time were constrained to be 16.13 ± 1.06 ka to 15.66 ± 0.92 ka, and 8630 ± 600 B.P. to 9561 ± 37 B.P.. From the data of Song J et al. (2013), Wang H et al. (2020), and Zhao YF et al. (2021), it can be inferred the south-central Jiali-Chayu fault zone may have experienced five paleoearthquake events since the Late Quaternary, which occurred at 16130–15660 years, 11060 ± 940 years, 8630–9561 B.P., 2780–2160 B.P., and 650 B.P., respectively, with a recurrence interval of about 2000–5000 years. The Late Quaternary slip rate of the Jiali-Chayu fault zone is still controversial. According to the GPS data (Song J et al., 2011; Wang M and Shen ZK, 2020; Zhang L et al., 2021), the central and southeastern segments of the Jiali-Chayu fault zone have a horizontal slip rate of 1.3–2.0 mm/a and 2–4 mm/a, and a compression rate of 2.5–2.9 mm/a and 5.1–6.2 mm/a (Table 3), respectively, indicating dextral and compression (Zhong N et al., 2021).

2.5. Lulang-Yigong fault zone

The Lulang-Yigong fault zone is located at the western boundary of the EHS, which is a juvenile strike-slip tectonic belt that cuts the Yarlung-Zangbo fault zone. The Lulang-Yigong fault consists of multiple diagonally distributed secondary faults, and some of its segments develop along the Yarlung-Zangbo fault zone. The Lulang-Yigong fault zone was active during the Early Cenozoic, followed by the Early-Middle Miocene, and underwent the last uplift during the Late Miocene (Dong HW et al., 2018). This fault zone has been struck by numerous earthquakes, the most active during the Holocene, and primarily subjected to sinistral strike-slip and tension components and has a vertical slip rate of about 0.17–0.27 mm/a (Xie C, 2018). The landforms along the Lulang-Yigong fault zone are dominated by deeply incised canyons and grooves on a slope or scarps (Figs. 12a, b). A third alluvial-proluvial terrace T3 has developed in the Lulang River in Sicun village, which offset by faults, forming a fault scarp with high continuity, and two small gullies on the terrace exhibit a synchronous sinistral offset of 6 m (Xie C, 2018). Through trenching across the fault scarp, Xie C (2018) revealed a faulting event that offset the Holocene gravel layer by up to 3.1 m. Lulang-Yigong fault zone also includes earthquake-induced SSDS (Figs. 12c, d), which are visible in Zhaxigang, Sicun, and Dongjiu villages along the Lulang-Yigong fault zone and include load structures, flame structures, liquefied deformation structures, and micro-faults (Wang HY et al., 2021). These SSDS are all interlaminar deformations with a small scale (2–10 cm), and most of them occur in the liquefiable clayey, silty sands and silty sand layers and are characterized by vertical repeatability and lateral continuity, which are mostly triggered by earthquakes (Zhong N et al., 2017, 2022a). From the OSL dating results, it can be concluded that the paleoearthquake events recorded in the lacustrine deposits in Dongjiu occurred before 19.58 ± 2.01 ka (Fig. 12d; Table 2). The trench on the terrace in northern Zhaxigang also revealed one paleoearthquake event, which occurred at 8640–5460 B.P. according to ^{14}C dating (Figs. 12e, f). Earthquake-induced liquefied diapir deformation structures have been discovered in the lacustrine

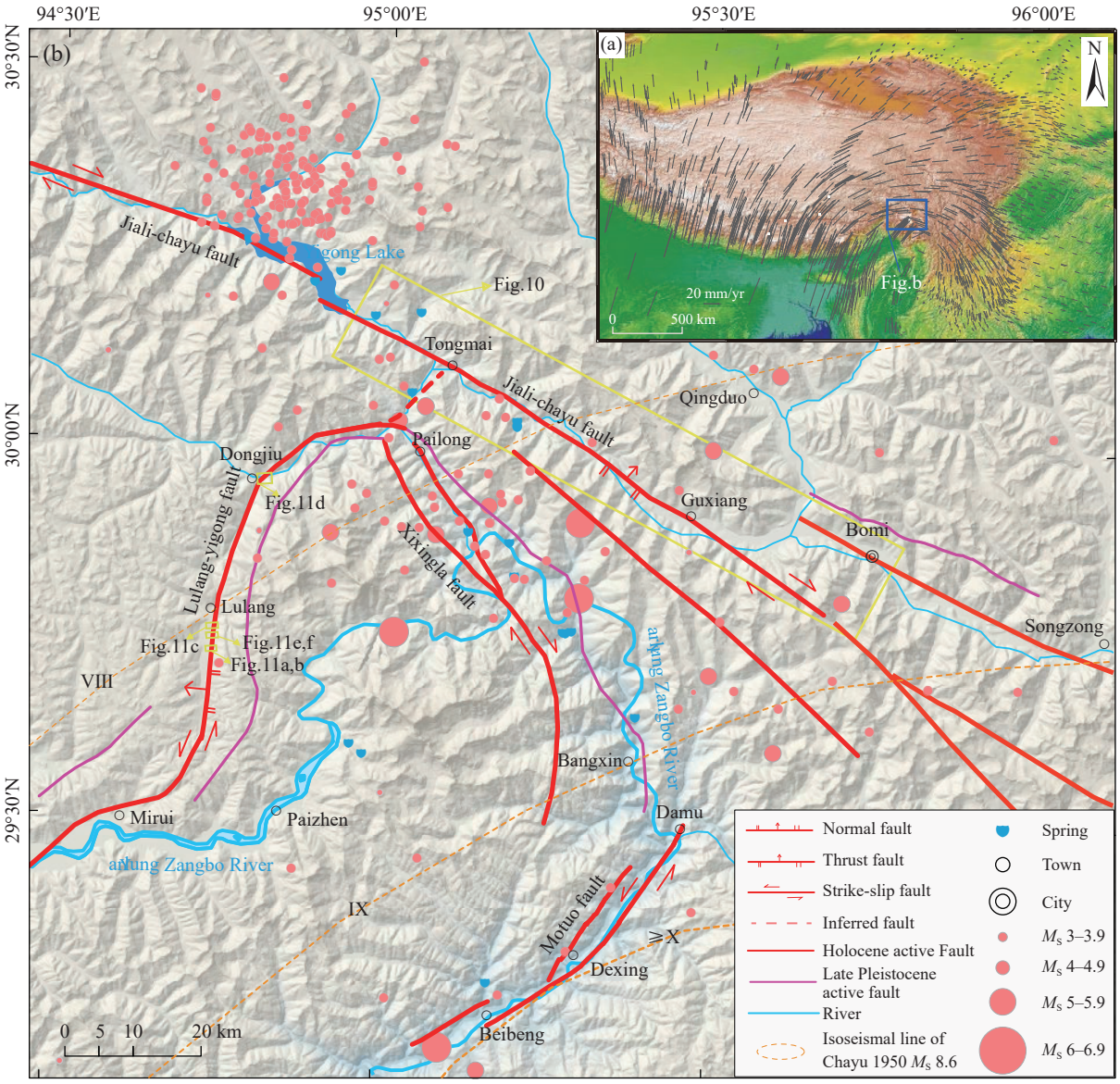

Fig. 10. a–GPS velocity fields of the horizontal crustal motion in Chinese continent in the relatively stable Eurasian Plate and its surrounding areas (after Wang M and Shen ZK, 2020); b–map of the geometric distribution in the Jiali-Chayu and Lulang-Yigong fault zones, the historical earthquakes in the EHS, and the isoseismal distribution of the 1950 Chayu M_S 8.5 earthquake (after You ZL et al., 1991).

deposits in Sicun village, possibly attesting to a paleoearthquake event of 8.8 ± 1.2 to 9.4 ± 0.5 ka (Wang HY et al., 2021). Interestingly, the south-central Jiali-Chayu fault zone also records a paleoearthquake event that occurred at 8630–9561 B.P. (Zhong N et al., 2021). Therefore, further research is needed to determine whether a major earthquake ($M_S \geqslant 8.0$) occurred in the EHS before 8 ka.

3. Regional fault activity and tectonic deformation patterns

3.1. Tectonic deformation patterns indicated by nature of active faults

According to the nature of the fault activities in the Ya'an-Linzhi section of the STTC, the faults in the Longmenshan (e.g. the Longmenshan and Daduhe fault zones) and those in the EHS (e.g. the Jiali-Chayu zone) primarily exhibit thrust motions. In contrast, faults in the Qiangtang block (e.g. the Yunongxi, Litang, Batang, Jinshajiang, Xiangdui-Luoni, Lancangjiang, Nujiang, and Bianba-Luolong fault zones) exhibit mainly strike-slip motions (Fig. 1; Table 1). As shown by the current tectonic deformation zoning of the TP (Fig. 13), a series of piedmont thrust fault zones formed in the EHS was obliquely subducted beneath the Indian Plate. Accordingly, the EHS is a strongly compressional uplift area where peaks with elevations exceeding 7000 m, such as the Namcha Barwa Peak and the Gyala Peri Peak have developed. Therefore, under rapid uplift and compression, the Jiali-Chayu fault zone exhibit dextral strike-slip and thrust components, while the Lulang-Yigong fault zone show sinistral strike-slip and tension components. Similarly, the collision and compression between the Bayan Har block and the Yangtze block in the east formed a series of imbricated thrust fault zones in the Longmenshan, and also a strongly compressional uplift area

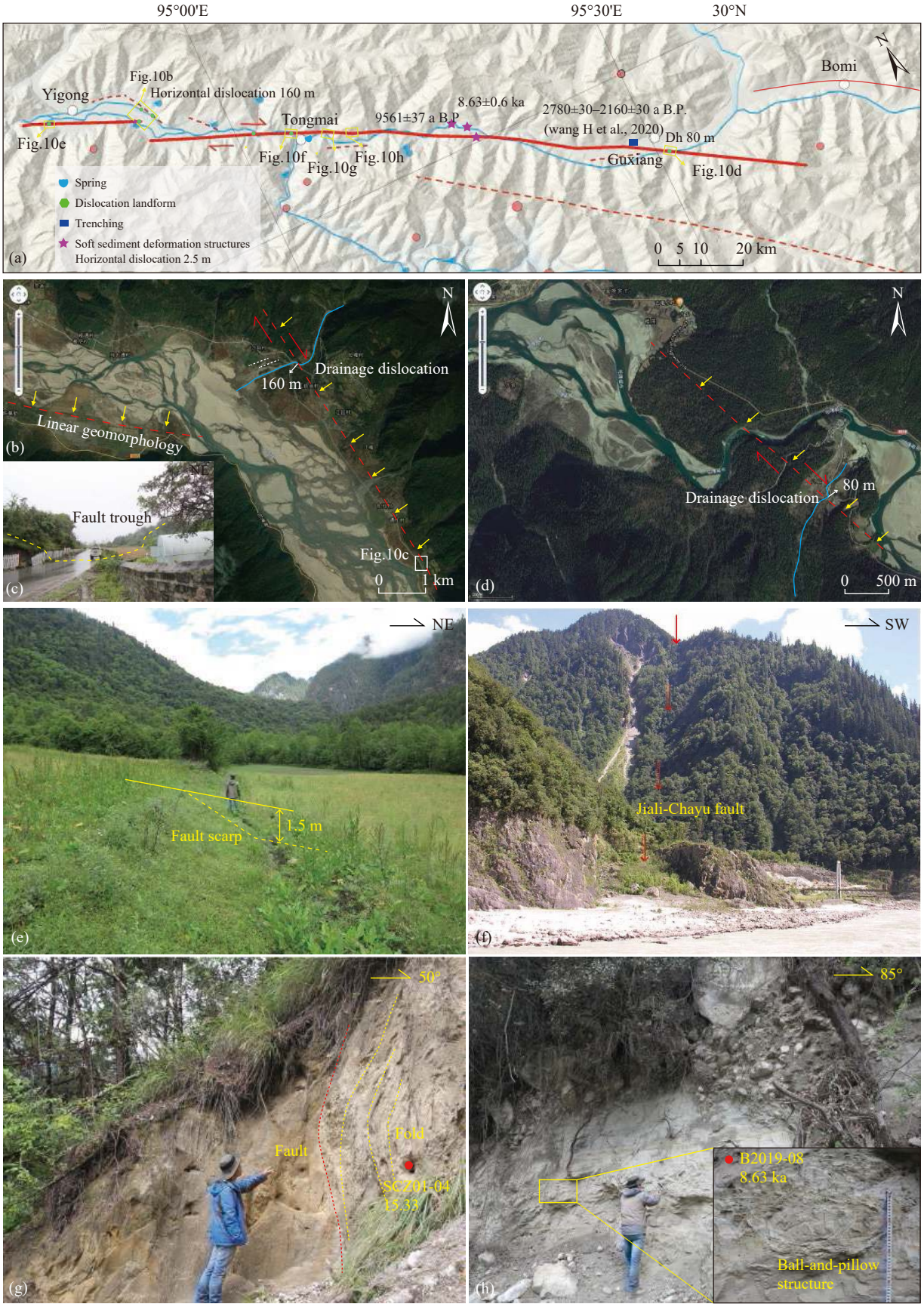

Fig. 11. a–Map of the spatial geometric distribution and offset landform characteristics in the middle segment of the Jiali-Chayu fault zone; b–d–maps of the drainage offset landforms in the Yigong and Guxiang lakes; c–a fault trough at Tongjia Village, Yigong; e–fault scarp in Gongde Village, Yigong; (f)–landforms near the Tongmai bridge (afte rSong J et al., 2013); g–h–maps of the deformation structures of typical soft sediments in lacustrine deposits in the Jialongba and Bitong villages.

Table 3. List of activity rate of Jiali-Chayu fault.

Reference	Fault property	Activity age	Sections	Activity rate/(mm/a)	
Armijo et al., 1989	Dextral	Late Quaternary		Horizontal	10–20
Ren JW et al., 2000	Dextral	Late Quaternary		Horizontal	4
Shen J et al., 2003	Dextral	Late Quaternary		Horizontal	<2–3
Meade, 2007	Dextral thrust	GPS		Horizontal	3
				Vertical	15
Tang FT et al., 2010	Dextral	GPS	West	Horizontal	4–6
			Middle	Horizontal	1–2
			Southeast	Horizontal	3–5
Song J et al., 2011	Dextral or sinistral thrust	GPS	West	Horizontal	4–5.8
			Middle	Horizontal	1.3–2.0
				Vertical	2.5
			Southeast	Horizontal	3.7–4.0
				Vertical	6.2
Zhu Z and Meng GJ, 2012	Dextral thrust	GPS		Horizontal	7.1±1
Langstaff and Meade, 2013		GPS		Horizontal	⩽2
Wang M and Shen ZK, 2020	Dextral	GPS		Horizontal	~3
Zhang L et al., 2021	Dextral	GPS	West	Horizontal	5.0±0.5
			Middle	Horizontal	2.4±0.8
			Southeast	Horizontal	3.8±0.9
Zhong N et al., 2021	Dextral thrust	Late Quaternary	West	Horizontal	2–4
			Middle	Horizontal	1.3–2.0
				Vertical	2.5–2.9
			Southeast	Horizontal	2.0–4.0
				Vertical	5.1–6.2

with significant topographic elevation differences. For instance, the horizontal distance between the Sichuan Basin with an altitude of 600 m and mountains with an altitude of over 5000 m within the plateau is less than 50 km (Zhong N et al., 2017b). The lateral extrusion area of the southeastern margin of the TP is also a tectonic zone formed by the rapid eastward extrusion of the Qiangtang block, which starts at a longitude of about 90°E in the west and is bounded by the Yushu-Xianshuihe and Jiali-Nujiang fault zones in the north and south, respectively (Han S et al., 2019). During the rapid eastward and southeastward migration of materials in the east of the Qiangtang block, the materials in the west are discontinuously driven eastward. As a result, many conjugated strike-slip faults and nearly-SN-trending normal faults were formed during the stretching process in the lateral extrusion area. The western and eastern Qiangtang blocks in this area show diffuse deformation and rigid block deformation, respectively (Li HB et al., 2021). Moreover, this area hosts many large rivers, such as Nujiang, Lancang, and Jinsha (Fig. 1), and consists primarily of deeply incised canyons or intermountain basins.

Based on the activities of the active fault zones, the current crustal deformation field revealed by GPS data, historical earthquakes, surface ruptures, and the types of focal mechanism solutions, Cheng J et al. (2012) subdivided the southeastern margin of the Tibet Plateau into 11 subblocks. The Litang fault zone is a boundary fault between the Yajiang and Zhongdian subblocks, and the Batang fault zone is a boundary fault between the eastern Qiangtang and Zhongdian subblocks. The eastward movement of the Qiangtang subblock was blocked by the Zhongdian subblock, generating significant compressive stress. As a result, the Batang fault zone should have certain thrust components, in addition to strike-slip components. This can be confirmed by the fact that the Jinshajiang fault zone to the south of Batang contains both strike-slip and thrust-slip components (Zhou RJ et al., 2007). It is noteworthy that the Litang fault zone exhibits significant segmentation, which a number of basins are distributed (Fig. 5). The Cuopuhu, Maoyaba, and Litang segments of the Litang fault zone show strike-slip and normal fault components, while the Kangga-Dawu segment contains strike-slip and thrust components (Chevalier ML et al., 2016). This result indicates that the Litang fault zone is not only controlled by the lateral extrusion-induced deformation structures at the southeastern margin of the TP, but also affected by the differential movement of the Yajiang and Zhongdian subblocks, and has complex tectonic deformations and tectonic assemblage patterns. Regionally, the NW-trending Litang fault zone (sinistral) and the NE-trending Batang fault zone (dextral) constitute an X-shaped conjugated fault system with strong EW-trending compressive stress. Seismic waveform data have also verified that the shear waves in the northwestern part of the rhombic Sichuan-Yunnan block show a polarization direction of nearly EW (Shi YT et al., 2013). Based on the above characteristics of active fault zones, Cheng J et al. (2012) considered that the compression between the eastern Qiangtiang and Yajiang subblocks and between the Yajiang and central Yunnan subblocks is the most significant at the southeast margin of the TP.

With the continuous compression of the Indian Plate

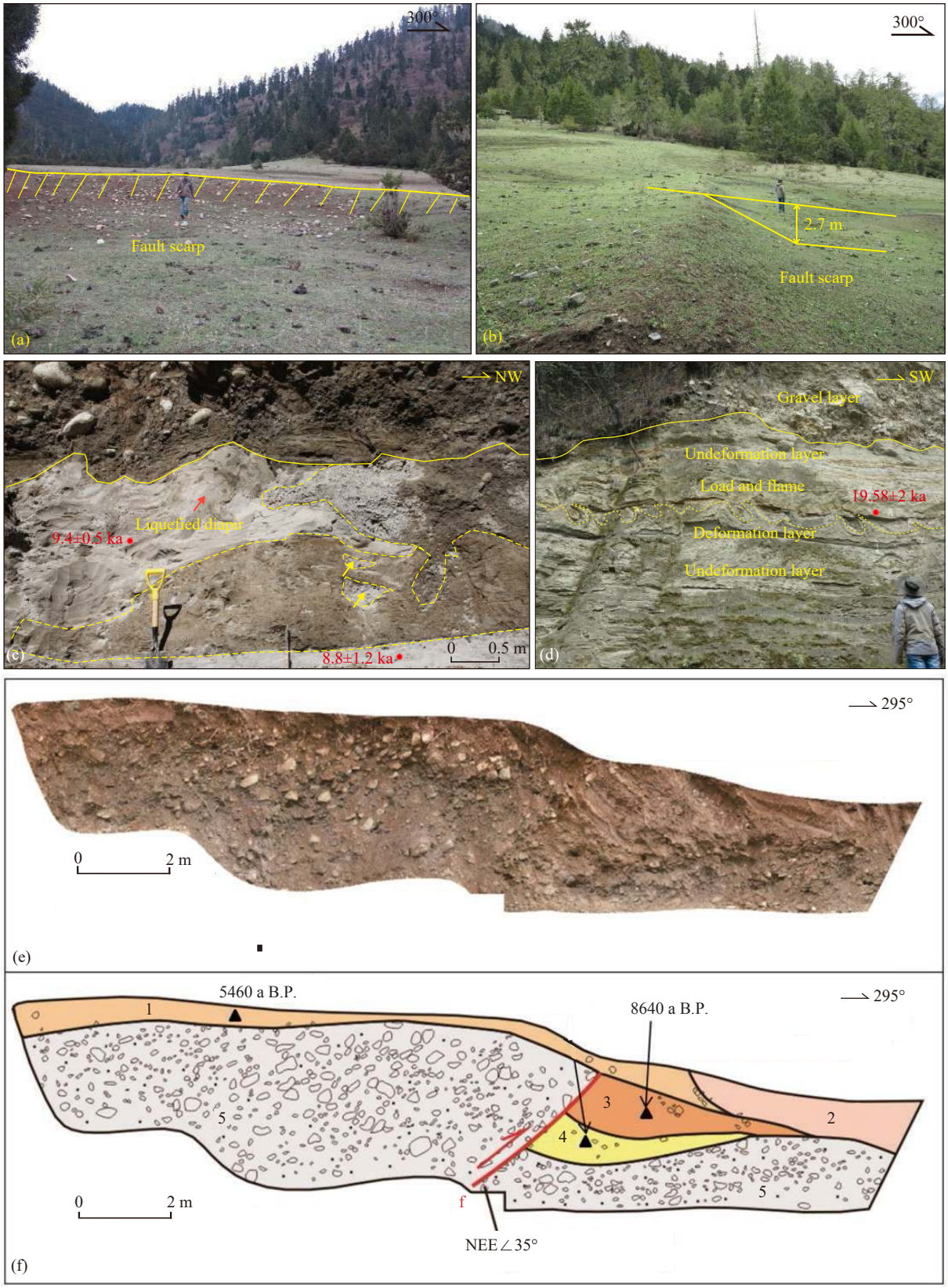

Fig. 12. a–b–Fault scarps developing in Zhaxigang Village, Lulang; c–d–Earthquake-induced soft sediment deformation structures in lacustrine deposits in the Sicun (after Wang HY et al., 2021) and Dongjiu villages, Lulang (this study); e–f–Sicun paleoearthquake trench (after Xie C, 2018).

toward the Eurasian Plate, the western and central parts of the Qiangtang block slowly shift and passively deform under the north-south compression and the eastward or southeastward traction of the materials in the east. Moreover, the upper crust in the eastern Qiangtang block escape and is extruded southeastward along the Xianshuihe fault zone and blocks

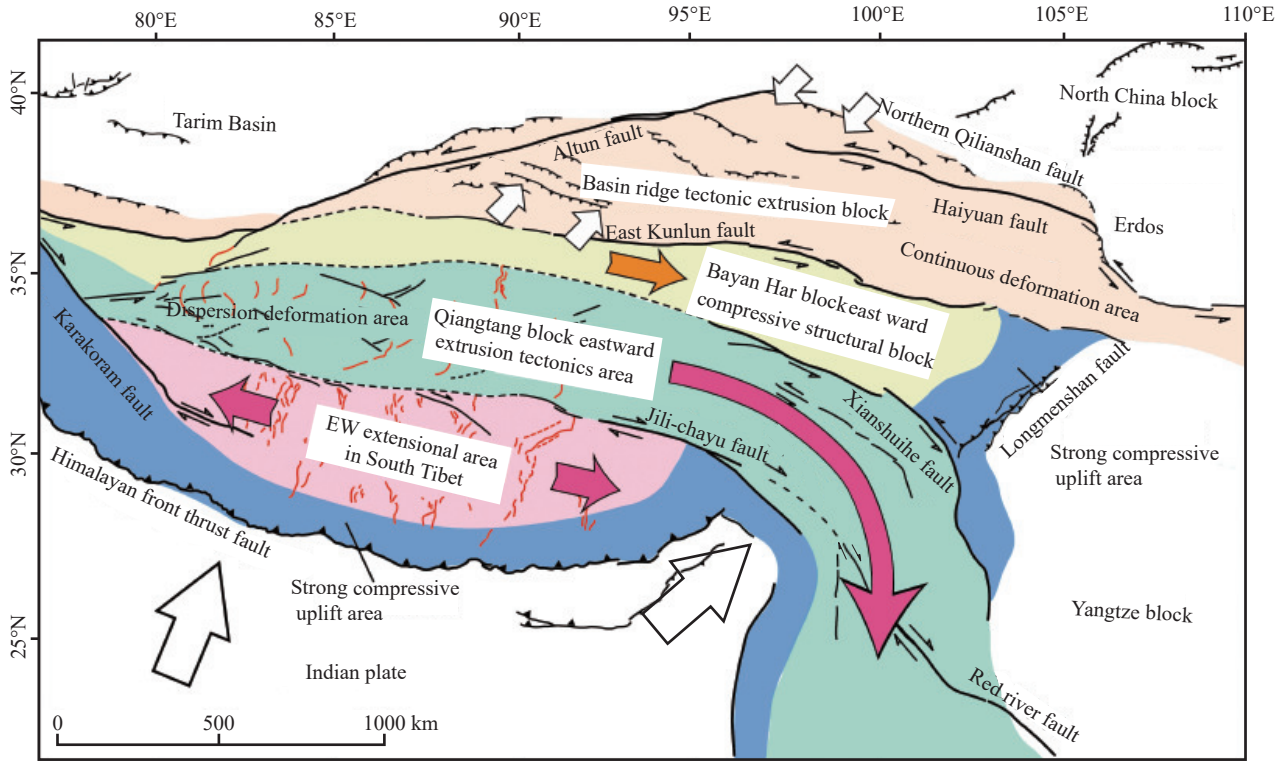

Fig. 13. Current tectonic deformation zoning of the Tibet Plateau (Li HB et al., 2021).

sandwiched by the Nujiang and Honghe fault zones, appearing as a rapidly extruded structure of rigid blocks (Leloup PH et al., 2007; Bai MK et al., 2018; Han S et al., 2019; Li HB et al., 2021). With the northward movement of the Indian Plate, a series of sinistral motions along NW-trending faults occurred within the TP. Moreover, the Kunlunshan-Xianshuihe fault zone divides the TP into the southern and northern blocks, with the southern block moving northward and northeastward. As a result, a northward, eastward, and southeastward fan-shaped radial pattern of the crustal movement centered on the TP was formed (Ding GY and Lu YC, 1986). During the northward movement of the Indian Plate, the blocks of the TP changed their direction and slipped toward the SSE direction since they were blocked by the Kunlunshan-Xianshuihe fault zone. Owing to the push force in the NNE direction from the Indian Plate, a thrust zone was generated at the margin of the plate, the Sagaing dextral shear zone was formed in the east, and then a push force in the NEE direction was generated in the TP. For example, in addition to strike-slip components, significant thrust components have been discovered in both the Nujiang fault zone (the Bangda fault) (Zhong N et al., 2022b) and the Lancangjiang fault zone (Ren JJ et al., 2022). As indicated by the focal mechanism solutions, the horizontal compressive stress in the NNE or NE direction from the Indian Plate controls the lithospheric stress field of the TP and its surrounding areas (Xu JR and Zhao ZX, 2006).

3.2. Tectonic deformation patterns and dynamics indicated by deep geophysics

Schoenbohm LM et al. (2005) suggested that the early tectonic deformation at the southeastern margin of the TP was mainly reflected in the lateral extrusion of the Indosinian block along the Ailaoshan fault zone, the rotation of the crust in the eastern TP drove the ductile flow of the lower crust, causing the Xianshuihe-Xiaojiang fault zone to active at 9–13 Ma. As a result, the upper crust rotated clockwise around the EHS, while the middle and lower crusts were extruded southeastward, leading to the decoupling between the upper and lower crusts (Schoenbohm LM et al., 2005). As indicated by broadband seismic surveys and magnetotelluric sounding, there may be east- and southeast-trending escape pathways of ductile, free-flowing materials at the southeastern margin of the TP (Jiang M et al., 2012). The magnetotelluric observations show that there indeed exist two weak material flows (low-resistivity anomaly zones) in the middle and lower crusts of the southeastern TP. One weak material flow extends eastward from the Lhasa block along the Yarlung Zangbo suture zone and then turns southward around the EHS, and the other extends southeastward from the Qiangtang block along the Jinshajiang and Xianshuihe fault zones and finally passes through the rhombic Sichuan-Yunnan block between the Xiaojiang and Honghe fault zones (Bai DH et al., 2010). The deep part of the southeastern TP is mainly characterized by the rapid plastic deformation of these two weak material flows, the brittle upper crust deformed and decoupled from the lower crust, with the upper crust primarily showing the strike-slip deformation of the blocks of the northern and southern boundary faults of the Maoyaba Basin in Litang (Bai DH et al., 2010). Based on the observational data of seismic arrays deployed in the southeastern TP, Liu QY et al. (2015) verified that the plateau spreads eastward through the flow of

lower crustal materials and the slip of the upper crust along fault blocks. Peng M et al. (2017) obtained images of the crustal structure below the EHS using the teleseismic receiver functions and the common conversion point (CCP) stacking imaging method, which shows the crustal uplift and thinning of the EHS and the presence of the partial melting in the crust are probably related to the upwelling of mantle-derived thermal materials, while the upwelling of the asthenospheric mantle may be caused by the rifting of the Indian Plate.

As revealed by the geometry and motion images of active structures, the sinistral strike-slip motions of the Xianshuihe fault zone at the northern boundary of the active Sichuan-Yunnan block were decomposed and absorbed by the nearly-SN-trending faults (e.g., the Anninghe and Daliangshan fault zones), leading to strong earthquake activity in these faults in the southeastern TP. Therefore, the southeastern margin of the TP has the following tectonic deformation characteristics: the collision between the Indian and Eurasian Plates and its aftereffects led to the strong uplift of the TP. As a result, the Sichuan-Yunnan block escaped (was extruded) in the SEE direction, which drove the middle and lower crustal flow and the rapid slip of large brittle faults in the upper crust in the southeastern TP, with strike-slip or thrust motions occurred. Given the significant rotation of the eastern TP, Yajiang, Zhongdian, and central Yunnan subblocks in the Sichuan-Yunnan block and the most significant compression among these subblocks, the extrusion of rigid blocks and gravitational slumping may coexist, which may be primarily caused by the dragging effect of the pipe flow in the lower crust (Cheng J et al., 2012). The middle and lower crusts on the western Sichuan Plateau have lower rheological intensities than normal crusts. Moreover, the differences in crustal thickness and landform elevation between the western Sichuan Plateau and its adjacent Sichuan Basin and South China block are up to 20–30 km and 3000–4000 m, respectively (Zhang PZ, 2008). All these allow for the formation of a lateral pressure difference, which could drive the flow of the weak layers in the middle and lower crusts. The lateral pressure difference may push the upper brittle crust cut by faults upward from the bottom, resulting in deformation and movement dominated by sinistral strike-slip motions, as well as strain accumulation and release on various faults, and strong earthquakes were formed. The deformation pattern transitioning from NWW-trending (e.g., the Xianshuihe fault zone) sinistral shear to nearly-NS-trending sinistral shear and compression is of significance across the China continent (Zhang PZ, 2008).

3.3. Tectonic deformation patterns indicated by geodetic survey

Based on 553 GPS observational data of the TP and its surrounding areas, Zhang PZ et al. (2004) concluded that the eastward extrusion of the TP is the clockwise rotation of crustal materials around the EHS under the push of the Indian Plate, the blocking of surrounding rigid blocks, and the current tectonic deformations are continuous. Chang LJ et al. (2015) found that the strike of the surface structures in the EHS is consistent with the movement trend of the GPS-derived surface movement velocity field. This finding indicates that the surface deformations in this zone are consistent with the deformations of the upper mantle, and the lithospheric deformations in this zone are vertical and consistent. Based on geological data and rock mechanical properties, Sun YJ et al. (2017) established a corresponding finite element numerical model, the results show that a series of arcuate faults with the EHS as the center of rotation in the southeastern TP exhibit the highest strain rate, relatively high slip rates (e.g., the Xianshuihe, Litang, Batang, and Jiali-Chayu fault zones), principal compressive stress with constantly varying direction, and dominant tensile stress, with active faults primarily exhibiting tensile and extrusive deformations. The results from GPS indicate that, relative to the stable Eurasian Plate, the internal materials of the TP rotate clockwise around the EHS when they migrate eastward as a whole, with the intensity of movement gradually increasing from north to south. Moreover, the TP has two boundary fault systems, namely Xianshuihe-Anninghe-Zemuhe-Xiaojiang fault zones system as the outer boundary and the Jiali-Chayu-Nujiang fault zones system as the inner boundary (Wang M and Shen ZK, 2020). In particular, the movement of crustal materials at the southeastern margin of the plateau shifts from the nearly-EW direction to the nearly-SN direction relative to the stable Eurasian Plate, exhibiting a lateral extrusion trend toward the southeast (Wang Q et al., 2001; Zhang PZ et al., 2004; Gan WJ et al., 2007; Liang SM et al., 2013; Wang M and Shen ZK, 2020).

4. Risk of future large earthquakes and disasters in the Ya'an-Linzhi section of the STTC

4.1. Large earthquake risk in the Ya'an-Linzhi section of the STTC

The Zheduotang fault was the seismogenic fault which triggered the 1955 Zheduotang M_S 7.5 earthquake, and the surface rupture was still clearly (Figs. 4b, c). Field investigations have found that two branches faults of the Zheduotang fault in the Zheduotang village, which forming a pull-apart structure (Fig. 4a). Through analysis of historical seismic gaps, current slip rates, Coulomb stress, frequent small earthquakes, tectonic stepover, and block boundary faults, it is confirmed that the Selaha-Kangding segment is a future strong earthquake risk zone. As a boundary fault of the Bayan Har and Sichuan-Yunnan blocks, the Xianshuihe fault zone has a slip rate of nearly 8–10 mm/a and a short earthquake recurrence interval, and its Sehala-Kangding segment is likely to undergo earthquakes of $M_S \geqslant 7$ in the future (Bai MK et al., 2018). The Litang and Batang fault zones are Holocene active faults which can trigger strong earthquakes, with the non-characteristic rupture behavior of the rupture events. The Litang and Batang fault zones are not only controlled by the lateral extrusion-induced deformation

structures at the southeastern margin of the TP, but also affected by the differential movement of the Yajiang and Zhongdian subblocks. Moreover, Litang and Batang fault zones earthquake activity tends to increase since the Holocene (Gao SP, 2021). In addition, it is worthwhile to further investigate the stress and strain distribution in the Litang fault zone, which is nearly parallel to the Xianshuihe fault zone, during the lateral extrusion of the southeastern margin of the TP and the clockwise rotation of the southeastern margin around the EHS.

Field investigations have found that there are two north-south branch faults in the middle-south segments of the Jiali-Chayu fault zone, characterized by dextral slip and thrust components (Fig. 10). The central and southeastern segments of the Jiali-Chayu fault zone have a horizontal slip rate of 1.3–2.0 mm/a and 2–4 mm/a, a compression rate of 2.5–2.9 mm/a and 5.1–6.2 mm/a, respectively, and the paleoearthquake recurrence interval of about 2000–5000 years. The Lulang-Yigong fault zone exhibits both sinistral slip and normal fault components, with a vertical slip rate of about 0.17–0.27 mm/a, and paleoearthquake events have occurred between 8630 to 9561 years and 8640 to 5460 years. The GPS monitoring data show that the Jiali-Chayu fault zone has a movement rate of 3–5 mm/a, and is currently in the locking stage (Zhang L et al., 2021). Therefore, there is a possibility of the occurrence of large earthquakes in Jiali-Chayu fault zone in the future (Tang FT et al., 2010; Wang XN et al., 2018). In particular, both the Jiali-Chayu (Zhong N et al., 2021) and Lulang-Yigong fault zones (Xie C, 2018) have low slip rates and a long earthquake recurrence interval. Earthquakes occur frequently near the EHS, such as the 2017 Milin M_S 6.9 earthquake and small earthquake swarms in Yigong Lake, Bomi (Fig. 10). Based on the analysis of GPS observational data and seismic data, Gupta TD et al. (2015) concluded that earthquakes with M_S 8.0 and above have a recurrence interval of about 200 years near the top of the EHS. Therefore, the earthquake activity of the EHS cannot be ignored. Currently, the top of the EHS is still subjected to high tectonic compression, and the metamorphic geological bodies continue to move northeastward, resulting in the shortening and deformation of blocks within the EHS, and the continuous accumulation of stress (Jiang M et al., 2012). As a result, there is a possibility that the Jiali-Chayu fault and Lulang-Yigong fault zones might undergo $M_S \geqslant 7$ earthquakes in the future. Therefore, the seismicity of the EHS and the Xianshuihe, Litang, and Batang fault zones cannot be ignored.

4.2. Earthquake disaster risk in the Ya'an-Linzhi section of the STTC

Large earthquakes or faults activities often trigger landslides, block rivers and form dammed lakes, subsequently, the dammed lakes break-out and cause flood disasters, and form a geological hazard chain risk (Xu C et al., 2014; Zhuang Y et al, 2020;Yang ZH et al., 2023), especially in active area on the southeastern TP. For example, the Mogangling landslide in Luding county induced by the 1786 Moxi M_S $7^3/_4$ earthquake blocked Dadu river and formed huge barrier lake (Yang ZH, et al., 2023). 1950 Chayu M_S 8.6 earthquake in the TP induced a large number of avalanche, ice collapse, rockfall and landslide disasters, and accumulated a large number of loose accumulation materials in the long and steep Guxiang gully of Bomi county, which seriously increased the development intensity and frequency of debris flow in the Guxiang gully (Yang ZH, et al., 2023). 1933 M_S 7.5 Diexi earthquake destroyed Diexi town, which induced many huge landslides blocked the Min River and formed several dammed lakes (Ren JJ et al., 2017). After two months, the break-out of dammed lakes killed at least 2500 peoples from Maoxian, Wenchuan, to Dujiangyan counties along the middle and lower reaches of the Min River (Tang RC et al., 1983). In 2018, two landslides happened successively on the right bank of the upper reaches of Jinsha River in Jinshajiang fault zone (Zhang YS et al., 2020), which dammed the river at Baige village, eastern TP. After the dammed lakes break-out, and their breaching flood brought about severe disaster to local residents and their production and life facilities along the river (Deng JH et al., 2019). Therefore, the Ya'an-Linzhi section of the STTC crossing (or nearby) this faults need to strengthen fault resistance, seismic design and earthquake disaster risk prevention, especially the Jinsha River and the Palong-Zangbu River.

In addition, the Ya'an-Linzhi section of the STTC is composed mostly of bedrock mountainous areas and deeply incised canyons. In particular, there is a lack of studies on the Batang, Jiali-Chayu and Lulang-Yigong fault zones, resulting in a small amount of paleoearthquake data, which hinder the understanding of the fault activity and the recurrence patterns of paleoearthquakes. More efforts should be paid to the application of new methods and techniques, especially high-precision InSAR, LiDAR, UAV (unmanned aerial vehicle) and GPS data, strengthen microseismic monitoring, to the investigation and evaluation of active faults in high-mountain valley areas, and it is necessary to enhance the identification and determination of paleoearthquake events recorded in lacustrine deposits in deeply incised canyons. Furthermore, also need analysis the current crustal deformation, stress distribution and fault activity patterns, clarify their relationship with large earthquakes, and determine the potential maximum magnitude, epicenters, and risk range.

5. Conclusions

(i) The Ya'an-Linzhi section of the STTC is from Ya'an, Kangding, Litang, Changdu, Bomi, to Linzhi, which is a high-risk area for earthquakes and geological disasters in the TP. At least 17 large earthquakes ($M_S \geqslant 7.0$) occurred in the Ya'an-Linzhi section of the STTC, and three large landslides (Mogangling landslide in Luding county induced by the 1786 Moxi M_S $7^3/_4$ earthquake; Yigong landslide in Bomi county and Baige landslide in Jiangda county) blocked river and formed huge barrier lake.

(ii) At least 13 active fault zones have developed in the

Ya'an-Linzhi section of the STTC, including 10 Holocene and three Late Pleistocene-Holocene active fault zones, and five faults zones (Xianshuihe, Litang, Batang, Jiali-chayu and Lulang-Yigong) have large threaten the safety of cities and major projects. The Xianshuihe and Jiali-Chayu fault zones are primarily controlled by the lateral extrusion of the southeastern margin of the TP and its clockwise rotation around the EHS. The Litang and Batang fault zones are not only controlled by the lateral extrusion-induced deformation structures at the southeastern margin of the TP but also affected by the differential movement of the Yajiang and Zhongdian subblocks.

(iii) Based on remote sensing images, ground surveys, and chronological tests, as well as the deep geophysical and current GPS data, the Selaha-Kangding segment of the Xianshuihe fault zone, the Maoyaba and Litang segment of the Litang fault zone, the middle segment (Yigong-Tongmai-Bomi) of Jiali-Chayu fault zone and Lulang-Yigong fault zone have the risk of experiencing strong earthquakes in the future, with a high possibility of the occurrence of $M_S \geqslant 7.0$ earthquakes. The Jinsha River and the Palong-Zangbu River, which is a high-risk area for geological hazard chain risk in the Ya'an-Linzhi section of the STTC.

(iv) More efforts should be paid to the application of new methods and techniques (InSAR, LiDAR, UAV, GPS et.), strengthen micro-seismic monitoring, and to the investigation and evaluation of active faults in high-mountain valley and bedrock areas. Strengthen analysis the current crustal deformation, stress distribution and fault activity patterns, clarify their relationship with large earthquakes, and determine the potential maximum magnitude, epicenters, and risk range. Engineering construction should avoid active fault as much as possible, and need to strengthen fault resistance, seismic design and earthquake disaster risk prevention.

CRediT authorship contribution statement

Ning-Zhong developed the writing-original draft, writing-Review and editing, visualization, project administration, funding acquisition. Changbao-Guo developed the methodology, investigation, writing review and editing. Xian-bing Zhang, Zhen Yang, Hao Yu mainly collected data. Rui-an Wu, Yang Wang and Hai-bing Li mainly discussing and editing. All authors contributed to the final version of the manuscript.

Declaration of Competing Interest

The authors declare no conflicts of interest.

Acknowledgements

The authors thank Professors Hao Zi-guo (editor), and two anonymous reviewers for valuable comments and the English improvement on an early version of the manuscript. The authors also thank Jia-wei Pan and Fu-cai Liu for assistance in the field. Special thanks the Luminescence Research Laboratory at National Institute of Natural Hazards, Ministry of Emergency Management of China for OSL dating. This work was supported by the National Natural Science Foundation of China (42177184), the Balance Research Funds of the Chinese Academy of Geological Sciences (60) and the China Geological Survey (DD20221816).

References

Armijo R, Tapponnier P, Han T. 1989. Late Cenozoic right-lateral strike-slip faultingin southern Tibet. Journal of Geophysical Research, 94(B3), 2787–2838. doi: 10.1029/JB094iB03p02787.

Bai D, Unsworth MJ, Meju MA, Ma X, Teng J, Kong X, Sun J, Wang L, Jiang C. 2010. Crustal deformation of the eastern Tibetan Plateau revealed by magnetotelluric imaging. Nature Geoscience, 3(5), 358–362. doi: 10.1038/ngeo830.

Bai MK, Chevalier ML, Leloup PH, Li HB, Pan JW, Replumaz A, Wang SG, Li KY, Wu Q, Liu FC, Zhang JJ. 2021. Spatial slip rate distribution along the SE Xianshuihe fault, eastern Tibet, and earthquake hazard assessment. Tectonics, 40(11), e2021TC006985. doi: 10.1029/2021TC006985.

Bai Mk, Chevalier ML, Li HB, Pan JW, Wu Q, Wang SG, Liu FC, Jiao LQ, Zhang JJ, Zhang L, Gong Z. 2022. Late Quaternary slip rate and earthquake hazard along the Qianning segment, Xianshuihe fault. Acta Geologica Sinica, 96(7), 2312–2332. doi: 10.3969/j.issn.0001-5717.2022.07.005.

Bai Mk, Chevalier ML, Pan JW, Replumaz, A, Leloup PH, Métois M, Li HB. 2018. Southeastward increase of the Late Quaternary slip-rate of the Xianshuihe fault, eastern Tibet. Geodynamic and seismic hazard implications. Earth and Planetary Science Letters, 485, 19–31. doi: 10.1016/j.epsl.2017.12.045.

Chang LJ, Wang CY, Ding ZF, You HC, Lou H, Shao CR. 2015. Upper mantle anisotropy of the eastern Himalayan syntaxis and surrounding regions from shear wave splitting analysis. Science China:Earth Sciences, 45(05), 577–588. doi: 10.1007/s11430-015-5098-2.

Chen LC, Wang H, Rang YK, Lei SX, Li X, Wu FY, Ma XQ, Liu CL, Han F. 2014. The 2013 Lushan M_S 7.0 earthquake:varied seismogenic structure from the 2008 Wenchuan earthquake. Seismological Research Letters, 85(1), 34–39. doi: 10.1785/0220130109.

Cheng J, Xu XW, Ma WT, Chen WT, Zhang Y. 2012. Block model and dynamic implication from the earthquake activities and crustal motion in the southeastern margin of Tibetan Plateau. Chinese Journal of Geophysics, 55(4), 1198–1212. doi: 10.6038/j.issn.0001-5733.2012.04.016.

Cheng J, Xu XW. 2018. Features of earthquake clustering from calculation of coulomb stress around the Bayan Har block, Tibetan Plateau. Seismology and Geology, 40(1), 133–154. doi: 10.3969/j.issn.0253-4967.2018.01.011.

Chevalier ML, Leloup PH, Replumaz A, Pan JW, Liu DL, Li HB. Gourbet L, Métois M. 2016. Tectonic geomorphology of the Litang fault system, SE Tibetan Plateau, and implication for regional seismic hazard. Tectonophysics, 682, 278–292. doi: 10.1016/j.tecto.2016.05.039.

Deng JH, Gao YJ, Yu ZQ, Xie HP. 2019. Analysis on the formation mechanism and process of Baige landslides damming the upper reach of Jinsha River, China. Advanced Engineering Sciences, 51(1), 9–16. doi: 10.29382/eqs-2020-0034.

Deng QD, Cheng SP, Ma J, Du P. 2014. Seismic activities and earthquake potential in the Tibetan Plateau. Chinese Journal of Geophysics, 57(7), 2025–2042. doi: 10.1002/cjg2.20133.

Deng QD, Gao X, Yang H. 2009. Fault block structure, active fault block structure and seismic activity. Geological Science, 44(04), 1083–1093.

Deng QD, Yu GH, Ye WH. 1992. Relationship Between Earthquake Magnitude and Parameters of Surface Ruptures Associated with Historical Earthquakes, Research on Active Fault (2). Beijing,

Seismological Press, 247–264 (in Chinese).
Ding GY, Lu YY. 1986. A preliminary study on the status of modern board sports in China. Science Bulletin, (18), 1412–141. doi: 10.1360/csb1986-31-18-1412.
Dong HW, Xu ZQ, Cao H, Li Y, Liu Z, Li HQ, Yi ZY, Chen X, Ma X, Wu C. 2018. Comparison of eastern and western boundary fault of eastern Himalayan syntaxis, and its tectonic evolution. Earth Science, 43(4), 933–951. doi: 10.3799/dqkx.2018.701.
Gai HL, Yao SH, Yang LP. 2021. Characteristics and causes of coseismic surface rupture triggered by the "5.22" M_S 7.4 earthquake in Maduo, Qinghai, and their significance. Journal of Geomechanics, 27(6), 899–912 (in Chinese). doi: 10.12090/j.issn.1006-6616.2021.27.06.073
Gan WJ, Zhang PZ, Shen Z, Niu Z J, Wang M, Wan YG, Zhou DM, Cheng J. 2007. Present-day crustal motion within the Tibetan Plateau inferred from GPS measurements. Journal of Geophysical Research: Solid Earth, 112, B08416. doi: 10.1029/2005JB004120.
Gao SP, Chen LH, Li YB, Wang H, Han MG, Feng JH, Lu LL, Peng SX, Jin C, Liu LT. 2022. Rupture Behavior of the Litang Fault within the Sichuan-Yunnan active block, southeastern Tibetan Plateau. Lithosphere, (Special 2), 8773676. doi: 10.2113/2022/8773676
Gao SP. 2021. Late quaternary paleo-seismology and faulting behavior of the internal and western boundary faults of northwest. Beijing, Institute of Geology, China Earthquake Administration, Ph. D thesis, 1–177 (in Chinese with English abstract).
Guo CB, Montgomery DR, Zhang Y, Zhong N, Fan C, Wu RA, Yan YQ. 2020. Evidence for repeated failure of the giant Yigong landslide on the edge of the Tibetan Plateau. Scientific Reports, 10(1), 1–7. doi: 10.1038/s41598-020-71335-w.
Guo CB, Wang BD, Liu JK, Tu JN, Zhang YS, Ma JF, Tie YB, Han B, Ma X, Liu F, Li X, Meng W, Zhong N, Yang ZH, Wu R. 2020. Main progress and achievements of the geological survey of the Sichuan-Tibet railway traffic corridor. China Geological Survey, 7(6), 1–12. doi: 10.19388/j.zgdzdc.2020.06.01.
Guo CB, Zhang YS, Montgomery DR, Du YB, Zhang GZ, Wang S. 2016. How unusual is the long-runout of the earthquake-triggered giant Luanshibao landslide, Tibetan Plateau, China? Geomorphology, 259, 145–154. doi: 10.1016/j.geomorph.2016.02.013.
Gupta T D, Riguzzi F, Dasgupta S, Mukhopadhyay B, Roy S, Sharma S. 2015. Kinematics and strain rates of the eastern Himalayan syntaxis from new GPS campaigns in northeast India. Tectonophysics, 655, 15–26. doi: 10.1016/j.tecto.2015.04.017.
Han MM. 2022. Late Quaternary Activity of the Bangda Segment along the Nujiang Fault Zone. Beijing, Institute of Geology, China Earthquake Administration, Ph. D thesis, 1–136 (in Chinese with English abstract).
Han S, Li HB, Pan JW, Lu HJ, Zheng Y, Liu DL, Ge CL. 2019. Co-seismic surface ruptures in Qiangtang terrane: insight into Late Cenozoic deformation of central Tibet. Tectonophysics, 750, 359–378. doi: 10.1016/j.tecto.2018.11.001.
Hong HC, Xu HB, Song F, Zhang XH. Li GH. 2013. Discussion on seismo-geological hazards induced by 2013 Lushan M_S 7.0 earthquake and its seismogenic fault. Acta Smologica Sinica, 35(5), 738–748. doi: 10.3969/j.issn.0253-3782.2013.05.012.
Jiang M, Peng M, Wang YX, Tan HD, Li QQ, Zhang LS, Wang W. 2012. Geophysical evidence for deep subduction of Indian lithospheric plate beneath eastern Himalayan syntaxis. Acta Petrologica Sinica, 28(6), 1755–1764.
Langstaff MA, Meade BJ. 2013. Edge-driven mechanical microplate models of strike-slip faulting in the Tibetan Plateau. Journal of Geophysical Research: Solid Earth, 118(7), 3809–3819. doi: 10.1002/jgrb.50272.
Leloup PH, Tapponnier P, Lacassin R, Searle MP. 2007. Discussion on the role of the Red River shear zone, Yunnan and vietnam, in the continental extrusion of SE Asia. Journal of the Geological Society, 164(6), 1253–1260. doi: 10.1144/0016-76492007-065.
Li DH, Ding ZF, Wu PP, Zheng C, Ye QD, Liang MJ. 2015. The deep seismogenic environment of the southeastern section of the Xianshuihe fault zone and the 2014 Kangding M_S 6.3 earthquake. Chinese Journal of Geophysics, 58(6), 1941–1953. doi: 10.6038/CJG20150610.
Li HB, Pan JW, Sun ZM, Si JL, Pei JL, Liu DL, Chevalier ML, Wang H, Lu HJ, Zheng Y, Li CR. 2021. Continental tectonic deformation and seismic activity: a case study from the Tibetan Plateau. Acta Geologica Sinica, 95(1), 194–213. doi: 10.3969/j.issn.0001-5717.2021.01.014.
Li HB, Wang ZX, Fu XF, Hou LW, Si JL, Qiu ZL, Li N, Wu FY. 2008. The surface rupture zone distribution of the Wenchuan earthquake (M_S 8.0) happened on May 12th, 2008. Geology in China, (5), 803–813 (in Chinese). doi: 10.3969/j.issn.1000-3657.2008.05.002.
Li TY, Du QF, You ZL, Zhang CG. 1995. Fault structure, movement mode and strong earthquake activity background of Xianshuihe fault zone. Journal of Geomechanics, (10), 165–171.
Li TS, Du QF, You ZL, Zhang CG. 1997. Risk assessment of Xianshuihe active fault zone and strong earthquake. Chengdu, Chengdu Cartographic publishing house, 1–129 (in Chinese).
Liang MJ, Yang Y, Du F, Gong Y, Sun W, Zhao M, He Q. 2020. Restudy on the Late Quaternary activity of the middle section of the Dari fault in Qinghai and the surface rupture zone of the 1947 M $7^3/_4$ earthquake. Seismology, 42(3), 703–714. doi: 10.3969/j.issn.0253-4967.2020.03.011.
Liang MJ. 2019. Characteristics of the Late-Quaternary Fault Activity of the Xianshuihe Fault. Beijing, Institute of Geology, China Earthquake Administration, Ph. D thesis, 1–125 (in Chinese with English abstract).
Liang SM, Gan WJ, Shen CZ, Xiao GR, Liu J, Chen WT, Ding XG, Zhou D. 2013. Three-dimensional velocity field of present-day crustal motion of the Tibetan Plateau derived from GPS measurements. Journal of Geophysical Research:Solid Earth, 118(10), 5722–5732. doi: 10.1002/2013JB010503.
Liu FS, Wu ZH, Yang ZY, Zhang YQ, Wang SB, Zhang H, Tong YB, Li HL. 2014. New progress and prospects of neotectonics and active tectonics synthetical study on eastern edge Qinghai-Xizang Plateau. Geological Bulletin of China, 33(4), 403–418. doi: 10.3969/j.issn.1671-2552.2014.04.002.
Liu K, Li YF, Guo HW, Zhang YF. 2021. Surface fracture characteristics and riedel shear structure analysis of the Litang M 7. 3 earthquake in West Sichuan in 1948. Acta Geologica Sinica, 95(8), 2346–2360.
Liu QY, Hilst VD, Li Y, Yao HJ, Chen JH, Guo B, Qi SH, Wang J, Huang H, Li SC. 2015. Eastward expansion of the Tibetan Plateau by crustal flow and strain partitioning across faults. Nature Geoscience, 7(5), 361–365. doi: 10.1038/ngeo2130.
Ma J, Zhou BG, Wang MG, An LK. 2020. Geological and geomorphological basis for Holocene activity in the northwest section of the fault zone of the Xianshuihe fault zone, the Zheduotang fault. Seismology and Geology, 42(5), 1021–1038. doi: 10.3969/j.issn.0253-4967.2020.05.001.
Meade B J. 2007. Present-day kinematics at the India-Asia collision zone. Geology, 35(1), 81–84. doi: 10.1130/G22924A.1.
Pan JW, Bai MK, Li C, Liu FC, Li HB, Liu DL, Chevalier ML, Wu KG, Wang P, Lu HJ, Chen P, Li CR. 2021. Coseismic surface rupture and seismogenic structure of the 2021–05–22 Maduo (Qinghai) M_S 7.4 earthquake. Acta Geologica Sinica, 95(6), 1655–1670. doi: 10.19762/j.cnki.dizhixuebao.2021166.
Pan JW, Li HB, Chevalier ML, Bai MK, Liu FC, Liu DL, Zheng Y, Lu HJ, Zhao ZB. 2020. A newly discovered active fault on the Selaha-Kangding segment along the SE Xianshuihe fault: the south Mugecuo fault. Acta Geologica Sinica, 94(11), 3178–3188. doi: 10.19762/j.cnki.dizhixuebao.2020196.
Peng JB, Cui P, Zhuang JQ. 2020. Challenges to engineering geology of Sichuan-Tibet railway. Chinese Journal of Rock Mechanics and Engineering, 39(12), 2377–2389. doi: 10.13722/j.cnki.jrme.2020.0446.
Peng M, Jiang M, Chen YI, Tan HD, Li QQ, Zhang LH, Xu LH. 2017. Crustal structure under the eastern Himalayan syntaxis seismic array and its geodynamic implications derived from receiver functions. Chinese Journal of Geophysics, 60(1), 70–85. doi: 10.6038/cjg20170107.

Peng C, Yin ZQ, Zhang XJ, Shao H, Pang MF. 2023. A comparative study of the main factors controlling geohazards induced by 10 strong earthquakes in Western China since the Wenchuan earthquake in 2008. China Geology, 6(1), 70–84. doi: 10.31035/cg2022009.

Ren J, Qi S, Xu Z, Kang W, Su Q, Lv Y. 2021. Timing of the Luanshibao giant landslide in eastern Tibet: the evidence from paleoseismology. Earth and Environmental Science, 861(5), 052002. doi: 10.1088/1755-1315/861/5/052002.

Ren JJ, Xu XW, Zhang SM, Yeats RS, Chen JW, Zhu AL, Liu S. 2017. Surface rupture of the 1933 M7.5 Diexi earthquake in eastern Tibet: implications for seismogenic tectonics. Geophysical Journal International, 212, 1627–1644. doi: 10.1093/gji/ggx498.

Ren JJ, Xu XW, Lv YW, Wang QX, Li A, Li K, Zhu JL, Cai JT, Liu S. 2022. Late Quaternary slip rate of the northern Lancangjiang fault zone in eastern Tibet: Seismic hazards for the Sichuan-Tibet Railway and regional tectonic implications. Engineering Geology, 306, 106748. doi: 10.1016/j.enggeo.2022.106748.

Ren JW, Shen J, Cao ZQ, Wang YP. 2000. Quaternary faulting of the Jiali fault, southeast Tibetan Plateau. Seismology and Geology, 22(4), 344–350.

Schoenbohm LM, Burchfiel BC, Chen LZ, Yin JY. 2005. Exhumation of the Ailao Shan shear zone recorded by Cenozoic sedimentary rocks, Yunnan province, China. Tectonics, 24(6), TC6015. doi: 10.1029/2005TC001803.

Shao ZG, Wu YQ, Ji LY, Diao FQ, Shi FQ, Li YJ, Long F, Zhang H, Zhu LG, Chen CY, Wang WX, Wei WX, Wang P, Liu XX, Liu Qi, Pan ZY, Yin XF, Liu YF, Wei, Z Y, Cao JL, Xu Jing, Han LB, Cheng J, Lu RQ, Xu YR, Li Xi, S XZ. 2022. Comprehensive determination for the late stage of the inter seismic period of major faults in the boundary zone of active tectonic blocks in Chinese mainland. Chinese Journal of Geophysics, 65(12), 4643–4658. doi: 10.6038/cjg2022P0489.

Shen J, Wang YP, Ren JW, Cao ZQ. 2003. Quaternary dextral shearing and crustal movement in southeast Tibetan Plateau. Xinjiang Geology, 21(1), 120–125. doi: 10.3969/j.issn.1000-8845.2003.01.019.

Shi YT, Gao Y, Zhang YJ, Wang H, Yao ZX. 2013. Shear-wave splitting in the crust in eastern Songpan-Garzê block, Sichuan-Yunnan block and western Sichuan basin. Chinese Journal of Geophysics, 56(2), 481–494. doi: 10.6038/cjg20130212.

Song J, Tang FT, Deng ZH, Cao ZQ, Zhou B, Xiao GR, Chen WT, Ge WP. 2011. Research on current movement characteristics and numerical simulation of main faults in the area around the eastern Himalayan tectonic knot. Chinese Journal of Geophysics, 54(06), 1536–1548. doi: 10.3969/j.issn.0001-5733.2011.06.013.

Song J, Tang FT, Deng ZH, Xiao GR, Chen WT. 2013. Late Quaternary movement characteristic of Jiali fault in Tibetan Plateau. Acta Scientiarum Naturalium Universitatis Pekinensis, 49(6), 973–980.

Sun YJ, Guo CB, Wu ZH, Fan TY, Li HL. 2017. Numerical study of the crustal stress, strain rate and fault activity in the eastern Tibetan Plateau. Acta Geoscientica Sinica, 38(3), 385–392. doi: 10.3975/cagsb.2017.03.08.

Tang C, Westen CJV. 2018. Atlas of Wenchuan earthquake geohazards: analysis of co-seismic and post-seismic geohazards in the area affected by the 2008 Wenchuan earthquake. Beijing, Science Press, 1–54.

Tang FT, Song J, Cao ZQ, Deng ZH, Wang M, Xiao GR, Chen WT. 2010. The movement characters of main faults around eastern Himalayan syntaxis revealed by the latest GPS data. Chinese Journal of Geophysics, 53(9), 2119–2128. doi: 10.3969/j.issn.0001-5733.2010.09.012.

Tang RC, Han WB. 1993. Sichuan active fault and earthquake. Beijing: Earthquake Press, 1–558 (in Chinese).

Tang RC, Liu, SL, Jiang, NQ. 1983. The 1933 Diexi Earthquake. Chengdu, Sichuan scientific and Technological Press, 69. (in Chinese).

Wang H, Li KJ, Chen LH, Chen XQ, Li An. 2020. Evidence for Holocene activity on the Jiali Fault, an active block boundary in the southeastern Tibetan Plateau. Seismological Research Letters, 91, 1776–1780. doi: 10.1785/0220190371.

Wang H, Wang P, Hu G, Ge Y, Yuan R. 2021. An early Holocene river blockage event on the western boundary of the Namche Barwa syntaxis, southeastern Tibetan Plateau. Geomorphology, 395, 107990. doi: 10.1016/j.geomorph.2021.107990.

Wang JT, Zhou, WJ, Dong, GC, Xian, F, Fu, YC, Zhang L, Tang L, Ding PK, Zhao, GQ. 2023. Timing and seismic origin of the historic Luanshibao rock avalanche in the Maoyaba basin, SE Tibetan Plateau: new evidence from ^{10}Be exposure-ages. Quaternary Geochronology, 75, 101430. doi: 10.1016/j.quageo.2023.101430.

Wang Q, Zhang PZ, Freymueller JT, Bilham R, Larson KM, Lai XA, You, XZ, Niu ZJ, Wu JS, Li YX, Liu JN, Yang, ZQ, Chen QZ. 2001. Present-day crustal deformation in China constrained by global positioning system measurements. Science, 294(5542), 574–577. doi: 10.1126/science.1063647.

Wang XN, Tang FT, Shao CR. 2018. The current movement characters of main faults surrounding the Namcha Barwa syntaxis. Technology for Earthquake Disaster Prevention, 13(2), 267–275. doi: 10.11899/zzfy20180202.

Wu WW, Wu P, Wei YL, Sun W. 2017. Regional characteristics of stress state of main seismic active faults in mid-northern part of Sichuan-Yunnan block. Chinese Journal of Geophysics, 60(5), 1735–1745. doi: 10.1002/cjg2.30043.

Wu ZH, Zhao GM, Long CX, Zhou CJ, Fan TY. 2014. The seismic hazard assessment around south-east area of Qinghai-Xizang Plateau: a preliminary results from active tectonics system analysis. Acta Geologica Sinica, 88(8), 1401–1416. doi: 10.3969/j.issn.0001-5717.2014.08.004.

Xiang W. 2023. Activity Characteristics and Seismic Risk Assessment of the Batang Fault in late Quaternary. Xi ’an, Chang ’an University, Master thesis, 1–76 (in Chinese with English abstract).

Xie C. 2018. Structural Geomorphology and Characteristics of Fault Activity in Namcha Barwa Area. Doctoral Degree Thesis. Beijing, Institute of Geology, China Earthquake Administration, Ph. D thesis, 1–136 (in Chinese with English abstract).

Xiong TY, Yao X, Zhang YS. 2010. A review on study of activity of Xianshuihe fault zone since the Holocene. Journal of Geomechanics, 16(2), 176–188. doi: 10.3969/j.issn.1006-6616.2010.02.007.

Xiong W, Tan K, Yu PF, Chen W. 2016. Triggering of Mw 5.9 Kangding earthquake by coulomb stress evolution along Xianshuihe fault Zone Since 1955. Geodesy and Geodynamics, 36(2), 95–100. doi: 10.14075/j.jgg.2016.02.001.

Xu C, Xu XW. Yao X, Dai, FC. 2014. Three (nearly) complete inventories of landslides triggered by the May 12, 2008 Wenchuan Mw 7. 9 earthquake of China and their spatial distribution statistical analysis. Landslides, 11(3), 441–461. doi: 10.1007/s10346-013-0404-6.

Xu J, Ji LY, Ji CW, Sun H, Zhao Q. 2017. Coulomb stress evolution and risk in the eastern boundary fault zone of the Sichuan-Yunnan rhombic block. Seismology and Geology, 39(3), 451–470. doi: 10.3969/j.issn.0253-4967.2017.03.002.

Xu JR, Zhao ZX. 2006. Regional stress field and tectonic movement characteristics of the Qinghai-Tibet Plateau and its surrounding areas. Geology in China, 33(2), 275–285. doi: 10.3969/j.issn.1000-3657.2006.02.005.

Xu XW, Wen XZ, Yu GH, Zheng RZ, Luo HY, Zheng B. 2005. The average slip rate, seismic rupture segmentation and recurrence characteristics of the Litang fault zone in western Sichuan. Scientia Sinica (Terrae), 33, 151–162 (in Chinese). doi: 10.3969/j.issn.1674-7240.2005.06.007.

Xu XW, Wu XY, Yu GH, Tan, XB, Li K. 2017. Seismo-geological signatures for identifying M ⩾7. 0 earthquake risk areas and their premilimary application in mainland china. Seismology and Geology, 39(2), 219–275. doi: 10.3969/j.issn.0253-4967.2017.02.001.

Yang ZH, Guo CB, Wu RA, Shao WW, Yu PF, Li CH. 2023. Potential seismic landslide hazard and engineering effect in the Ya’an-Linzhi section of the Sichuan-Tibet transportation corridor, China. China Geology, 6, 228–240. doi: 10.31035/cg2023032.

Yang ZH, Guo CB, Wu RA, Zhong N, Ren SS. 2021. Predicting seismic

landslide hazard in the Batang fault zone of the Qinghai-Tibet Plateau. Hydrogeology & Engineering Geology, 48(5), 91–101. doi: 10.16030/j.cnki.issn.1000-3665.202009024.

Yi GX, Long F, Wen XZ, Liang MJ, Wang SH. 2015. Analysis of seismogenic structure of Kangding M_S 6.3 earthquake sequence on November 22. Chinese Journal of Geophysics, 58(04), 1205–1219. doi: 10.6038/cjg20150410.

You ZL, Wu ZX, Xie LJ. 1991. Intensity distribution of the magnitude 8.6 earthquake in Chayu, Tibet. Journal of Disaster Prevention and Mitigation, 0(1), 94–102(in Chinese).

Zeng QL, Yuan, GX, Davies, T., Xu B, Wei, RQ, Xue, XY, Zhang, LQ. 2020. ^{10}Be dating and seismic origin of Luanshibao rock avalanche in SE Tibetan Plateau and implications on Litang active fault. Landslides, 17, 1091–1104. doi: 10.1007/s10346-019-01319-z.

Zhan Y, Liang M J, Sun XY, Huang FP, Zhao LQ, Gong Y, Han J, Li CX, Zhang PZ, Zhang HP. 2021. Deep structure and seismogenic pattern of the 2021.5.22 Madoi (Qinghai) M_S 7.4 earthquake. Chinese Journal of Geophysics, 64(7), 2232–2252. doi: 10.6038/cjg2021O0521.

Zhang D, Wu ZH, Li JC, Liu ST, Ma D, Lu Y. 2019. The delineation of three-dimensional shallow geometry of active fault based on TLS and GPR: a case study of an normal fault on the north margin of Maoyaba basin in Litang, western Sichuan province. Seismology and Geology, 41(02), 130–152. doi: 10.3969/j.issn.0253-4967.2019.02.008.

Zhang KQ, Wu ZH, Zhou CJ, Tian TT, Li YH, Li JC. 2020. Paleoearthquake events and in homogeneous activity characteristics in the Benge-Cunge section of the Litang fault zone in the western Sichuan province. Acta Geologica Sinica, 94(4), 1295–1303. doi: 10.19762/j.cnki.dizhixuebao.2020025.

Zhang L, Liang S, Yang X, Gan W, Dai C. 2021. Geometric and kinematic evolution of the Jiali fault, eastern Himalayan syntaxis. Journal of Asian Earth Sciences, 212, 104722. doi: 10.1016/j.jseaes.2021.104722.

Zhang L, Zhou YJ, Zhang X, Zhu AY, Li B, Wang SG, Liang SS, Jiang C, Wu JP, Li YX, Su JR, Yan LJ, Fang LH. 2022. The 2022 Luding M_S 6.8 earthquake in Sichuan: An intracontinental strong earthquake that filled the seismic gap. China Science, Earth Science, (accepted) (in Chinese).

Zhang PZ, Shen ZK, Wang M, Gan WJ. 2004. Kinematics of present-day tectonic deformation of the Tibetan Plateau and its vicinities. Seismology and Geology, (03), 367–377. doi: 10.3969/j.issn.0253-4967.2004.03.002.

Zhang PZ. 2008. Current tectonic deformation, strain distribution and deep dynamic processes in the western Sichuan region on the eastern edge of the Qinghai-Tibet Plateau. Scientia Sinica (Terrae), 09, 1041–1056. doi: 10.1360/zd2008-38-9-1041.

Zhang YS, Ba RJ, Ren SS, Li ZL. 2020. An analysis of geo-mechanism of the Baige landslide in Jinsha River, Tibet. Geology in China, 47(6), 1637–1645. doi: 10.12029/gc20200603.

Zhang YS, Ren SS, Liu XY, Guo CB, Li JQ, Bi JB, Ran LN. 2023. Reactivation mechanism of old landslide triggered by coupling of fault creep and water infiltration: a case study from the east Tibetan Plateau. Bulletin of Engineering Geology and the Environment, 82(8), 291. doi: 10.1007/s10064-023-03290-5.

Zhang YZ, Replumaz A, Wang GC, Philippe HL, Cécile G, Matthias B, Peter, van der B, Jean LP, Wang A, Zhang KX, Marie LC, Li HB. 2015. Timing and rate of exhumation along the Litang fault system, implication for fault reorganization in southeast Tibet. Tectonics, 34(6), 1–25. doi: 10.1002/2014TC003671.

Zhao GH. 2014. Study on the Activity and Tectonic Geomorphology of Litang Fault in the Sichuan-Yunnan Block. Chengdu, Chengdu University of Technology, Master thesis, 1–86 (in Chinese with English abstract).

Zhao YF, Gong WB, Jiang W, Chen LY, Qiu DW. 2021. Multi-stage characteristics and tectonic significance of the Jiali Fault in Guxiang-Tongmai section, south Tibet. Geoscience, 35(1), 220–233. doi: 10.19657/j.geoscience.1000-8527.2021.010.

Zhong N, Guo CB, Huang XL, Wu RA, Ding YY, Zhang XB, Li HB. 2021. Late Quaternary activity and paleoseismic records of the middle south section of the Jiali-Chayu fault. Acta Geologica Sinica, 95(12), 3642–3659. doi: 10.3969/j.issn.0001-5717.2021.12.005.

Zhong N, Jiang HC, Li HB, Su DC, Xu HY, Liang LJ, Fan JW. 2022a. The potential of using soft-sediment deformation structures for quantitatively reconstructing paleo-seismic shaking intensity: progress and prospect. Environmental Earth Sciences, 81(16), 1–22. doi: 10.1007/s12665-022-10504-8.

Zhong N, Jiang HC, Li HB, Xu HY, Huang XL. 2020. The genetic types of soft sediment deformation structures and their characteristics in the fluvial-lacustrine sediments, eastern Tibetan Plateau. Acta Geoscientica Sinica, 41(1), 23–36. doi: 10.3975/cagsb.2019.102302.

Zhong N, Jiang HC, Xu HY, Peng XP. 2017a. Paleoearthquake researches via soft sediment deformation of load, ball-and-pillow structure: a review. Geological Review, 63(3), 719–738. doi: 10.16509/j.georeview.2017.03.013.

Zhong N, Yang Z, Zhang XB, Ding YY, Wu RA, Wang Y, Guo CB, Li HB. 2022b. Evidence of Holocene activity and paleoseismic records in the central section of Bangda fault in Nujiang fault zone. Geological Review, 68(6), 2021–2032. doi: 10.16509/j.georeview.2022.08.131.

Zhong N, Song X, Xu H, Jiang H. 2017b. Influence of a tectonically active mountain belt on its foreland basin: evidence from detrital zircon dating of bedrocks and sediments from the eastern Tibetan Plateau and Sichuan basin, SW China. Journal of Asian Earth Sciences, 146, 251–264. doi: 10.1016/j.jseaes.2017.05.035.

Zhong N. 2017. Earthquake and Provenance Analysis of the Lacustrine Sediments in the Upper Reaches of the Min River During the Late Pleistocene. Beijing, Institute of Geology China Earthquake Administration, Ph. D thesis, 1–181 (in Chinese with English abstract).

Zhou CJ, Wu ZH, Zhang KQ, Li JC, Jiang Y, Tian TT, Liu YH, Huang XJ. 2015. New chronological constraint on the co-seismic surface rupture segments associated with the Litang fault. Seismology and Geology, 37(2), 455–467. doi: 10.3969/j.issn.0253-4967.2015.02.009.

Zhou RJ, Chen GX, Li Y, Zhou ZH, Gong Y, He YL, Li XG. 2005. Research on active faults in Litang-Batang region, western Sichuan province, and the seismogenic structures of the 1989 Batang M_S 6.7 earthquake SW arm. Eismology and Geology, (1), 31–43.

Zhou RJ, Lei JC, Li XG, Yang T. 2000. Geology and geomorphic evidence for activity of Daduhe Fault since late Quaternary // CHEN Yuntai (ed). Collection of Essays for the 8th Academic Conference of the Seismological Society of China. Beijing Seismological Press, 54 (in Chinese).

Zhou RJ, Ye YQ, Li Y, Li XG, He YL, Ge TY. 2007. Late Quaternary active of the Shawan of the Litang faults. Quaternary Sciences, 27(1), 45–53.

Zhou RJ. 2014. 1∶50000 banded active fault mapping of Litang-Yidun fault. Sichuan Earthquake Administration,1–72.

Zhou RJ, Liu S, Li Y, Liang MJ, Wang SY, Yan ZK. 2016. Earthquake surface rupture and recurrence interval of large earthquakes in the Damaoyaba-Litang section of the Litang fault. Proceedings of the annual meeting of the China Geoscience Association, 677–678 (in Chinese).

Zhu Z, Meng GJ. 2012. An analysis of fault activity in shear zone at low latitudes from GPS measurements. Journal of Geodesy and Geodynamics, 32, 26–30. doi: 10.3969/j.issn.1671-5942.2012.01.007.

Zhuang Y, Yin YP, Xing AG, Jin, KP. 2020. Combined numerical investigation of the Yigong rock slide-debris avalanche and subsequent dam-break flood propagation in Tibet, China. Landslides, (6), 2217–2229. doi: 10.1007/s10346-020-01449-9.